Joint Angle Estimation and Signal Reconstruction for Coherently Distributed Sources in Massive MIMO Systems Based on 2-D Unitary ESPRIT

YUAN ZHOU[1], ZESONG FEI[1], (Senior Member, IEEE), SHAOSHI YANG[1], (Member, IEEE), JINGMING KUANG[1], SHENG CHEN[2,3], (Fellow, IEEE), AND LAJOS HANZO[2], (Fellow, IEEE)

[1]School of Information and Electronics, Beijing Institute of Technology, Beijing 100081, China
[2]School of Electronics and Computer Science, University of Southampton, Southampton SO17 1BJ, U.K.
[3]King Abdulaziz University, Jeddah 21589, Saudi Arabia

Corresponding author: Zesong Fei (feizesong@bit.edu.cn)

ABSTRACT We consider the challenging problem of joint angle estimation and signal reconstruction for coherently distributed (CD) sources in massive multiple-input–multiple-output (MIMO) systems employing uniform rectangular arrays. A simplified method inspired by the two-dimensional (2-D) unitary estimating signal parameters via rotational invariance technique (ESPRIT) is proposed to estimate both the central angle and the angular spread without the need for a spectrum peak search and covariance matrix matching process. We first approximate the 2-D generalized steering vector expressed as a Schur-Hadamard product by a pair of one-dimensional generalized steering vectors. Then, we obtain two approximate rotational invariance relationships with respect to the central angles of the CD sources using a linear approximation of the individual generalized steering vectors of the azimuth and elevation subarrays. With the aid of this approximate decomposition, a new unitary ESPRIT-inspired algorithm is conceived to automatically pair the 2-D central angle estimations and a novel method capable of bypassing the high-complexity search process is proposed for angular spread estimation. Furthermore, the closed-form approximate Cramer-Rao lower bounds are derived for the estimators of both the central angles and the angular spreads. The complexity of the proposed estimator is also analyzed. Additionally, the orthogonality of the generalized steering vectors is proved, which enables us to propose a low-complexity method to reconstruct the CD signal matrix by replacing the inversion operator with the conjugate transpose operator. The simulation results demonstrate the efficiency of our proposed approach.

INDEX TERMS Massive multiple-input multiple-output, two-dimensional array, coherently distributed source, direction-of-arrival, angular spread, signal reconstruction.

I. INTRODUCTION

The explosive growth of high-rate multimedia wireless services driven by smart phones and the mobile Internet has motivated the investigation of the fifth-generation (5G) cellular network. The new 5G network will enjoy superior spectral and energy efficiency compared with the existing 4G systems. The improvements mainly arise from the adoption of several new enabling techniques, including millimeter-wave communications, device-to-device communications, cloud-based radio access networks and massive multiple-input multiple-output (MIMO) solutions [1]–[3]. The massive MIMO techniques, which rely on a large number of antennas at each base station (BS), provide a high degree of spatial freedom to substantially enhance the system's throughput, energy efficiency and link reliability [4], [5]. For massive MIMO systems, direction-of-arrival (DOA) estimation is particularly important, since it is an essential piece of knowledge for the BS to perform beamforming in many scenarios, such as in millimeter-wave bands or for frequency-division duplex (FDD) based systems.

The problem of DOA estimation has been the focus of research for decades [6], and numerous powerful methods have been developed, such as maximum-likelihood (ML) spectral estimation [7], multiple signal

classification (MUSIC) [8], root-MUSIC [9], estimating signal parameters via rotational invariance technique (ESPRIT) [10] and unitary ESPRIT techniques [11]. More recently, DOA estimation algorithms have also been conceived for massive MIMO systems [12]–[21]. However, all the contributions in [7]–[18] assumed that the received signals originate from far-field point sources, which gives rise to perfectly planar wavefronts impinging on the array with discrete and fixed DOAs. In practical environments, such as wireless communications, radar and navigation, the transmitted signals are often obstructed by buildings, vehicles and trees and/or reflected by rough surfaces. Thus, an antenna array often receives multi-path signals, which have passed through a number of scatterers. Therefore, depending on the nature of reflection and scattering, using a spatially-distributed-source-based model may be more appropriate [22]. Furthermore, depending on the relationship between the channel's coherence time and the observation period, the signal components arriving from different directions exhibit varying degrees of correlation, ranging from totally uncorrelated (incoherent) to fully correlated (coherent) [23]. If the channel's coherence time is much shorter than the observation period, all the signals arriving from different directions can be assumed to be uncorrelated, and hence an incoherently distributed (ID) model becomes relevant. By contrast, in the case of coherently distributed (CD) sources, the signal components arriving from different directions can be regarded as some form of replicas of the same signal [24].

Several methods have been proposed to estimate both ID and CD sources. Parameter estimators were proposed for one-dimensional (1D) localization of ID sources in [23] and [25]–[29], where only the azimuth angular parameters need to be estimated. Most of these estimators can be extended to the two-dimensional (2D) scenario, where both the azimuth and elevation angular parameters have to be estimated. Among the existing approaches conceived for 2D DOA estimation of ID sources, the ML estimator of [25] is optimal but imposes excessive complexity. The approximate ML estimator of [26] is suboptimal, but it has lower complexity. To further reduce the complexity, least-squares (LS) estimators using covariance matrix matching were proposed in [27]–[29]. Moreover, the DOA estimation of 2D ID sources in the context of uniform rectangular array (URA) and uniform cylindrical array based massive MIMO systems were solved in [19] and [20], respectively. Note that in most cellular radio systems, the BS antennas are mounted on a tower, which can be far from potential multipath generators in the channel. It is quite common that the scatterers are local to UEs and the BS is sufficiently far away, and thus the scattered signals arriving from a given UE will be coherent and confined to a relatively small angular range [30]. Hence, the study of DOA estimation for CD sources in massive MIMO systems is necessary. The work [21] for the DOA estimation of CD sources in massive MIMO systems only considered 1D localization with the aid of a uniform linear array (ULA). However, owing to the limited space at the BS, massive MIMOs are most likely to employ 2D arrays in a plane, such as URA, in order to accommodate a large number of antenna elements, leading to a 2D DOA estimation problem. The 2D DOA estimation of each CD source has four angular parameters: the central azimuth DOA, central elevation DOA, azimuth angular spread and elevation angular spread.

In the literature, several DOA estimation techniques [31]–[35] have been presented for 2D CD sources by considering L-shaped linear arrays or uniform circular arrays (UCA). Specifically, for the UCA based system, the search for the four parameters of each CD source was decomposed into two search procedures, each responsible for estimating only two parameters of the given CD source [31], [32]. A similar transformation of the search procedure was performed for systems based on the L-shaped linear arrays [33]. These estimators rely on a spectrum peak search and their associated computational complexities are very high. Employing two parallel UCAs and exploiting the relationship between the signal subspace and the steering vector, a sequential one-dimensional searching (SOS) algorithm was proposed in [34] to estimate the central azimuth DOA or the central elevation DOA of each CD source, which reduces the computational cost, but it did not consider the estimation of angular spreads. Zheng *et al.* [35] studied the estimation of the central azimuth and elevation DOAs for a system employing three parallel ULAs, but they also did not consider the estimation of the angular spreads. The conventional distributed signal parameter estimator (DSPE) proposed in [22] for a ULA can be extended to the URA case to estimate both the central angles and the angular spreads. However, it relies on a high-complexity spectrum peak search. The ESPRIT-like DOA estimators, such as [10] and [19], cannot be used directly to estimate the 2D CD sources of massive MIMO systems. To the best of our knowledge, there are no studies that can efficiently estimate the central azimuth and elevation DOAs as well as the azimuth and elevation angular spreads of CD sources for the massive MIMO systems employing a URA. Given the superior capacity of URA compared with UCA [36], [37], this is an important research topic.

Signal reconstruction for the massive MIMO system associated with CD sources is another important and challenging problem, and yet there is a paucity of research in this area. Standard LS signal matrix reconstruction requires the Moore-Penrose pseudo-inverse of the array's steering matrix, which is extremely challenging for massive MIMO systems. The authors of [11] proposed a method of reconstructing the signal matrix without requiring the inverse of the array steering matrix. However, the method was proposed to estimate point sources and its performance is not attractive for estimating CD sources. To the best of our knowledge, there is no research that explicitly addresses signal reconstruction for 2D CD sources in massive MIMO systems employing URA.

With the above background, in this paper, we consider the challenging problem of joint angle estimation and signal

reconstruction for 2D CD sources in massive MIMO systems employing a URA. Our contributions are as follows.

- We transform the 2D generalized steering vector approximately into the Kronecker product of two 1D generalized steering vectors and obtain a pair of approximate rotational invariance relationships with respect to the central DOAs of CD sources by using a linear approximation. With the aid of this approximate decomposition, the conventional ESPRIT [10] becomes applicable in both the azimuth and elevation directions for central angle estimation, while imposing lower complexity than the DSPE. However, the conventional ESPRIT requires pair matching between the azimuth and elevation angle estimations, which requires additional computational load, and it cannot be used for angular spread estimation.

- Based on the above-mentioned approximate decomposition, a 2D unitary ESPRIT-based algorithm is proposed, which automatically pairs the 2D central angle estimation and imposes significantly lower complexity than the conventional ESPRIT at the cost of a modest degradation in estimation accuracy. Furthermore, a new low-complexity method is proposed for angular spread estimation without the need for spectrum peak search, while maintaining satisfactory performance.

- In addition, the closed-form approximate Cramér-Rao lower bound (CRLB) is derived for the proposed estimator of central angles and angular spreads, and the complexity of the proposed estimator is compared with that of the conventional DSPE.

- By proving the orthogonality of the generalized steering vectors, a low-complexity method is proposed to reconstruct the CD signal matrix, replacing the high-complexity inversion operator with the conjugate transpose operator, which has a much lower complexity.

Throughout the paper, lower-case and upper-case boldface symbols denote vectors and matrices, respectively. $\mathbf{I}_K$ is the $K \times K$ identity matrix, and $\mathbf{0}$ is the zero matrix with appropriate dimensions. $[\cdot]_{p,q}$ denotes the (p, q)th entry of a matrix, and $[\cdot]_p$ is the pth element of a vector. The Kronecker product and Hadamard product operators are given by $\otimes$ and $\odot$, respectively, while $(\cdot)^*$, $(\cdot)^T$, $(\cdot)^H$ and $(\cdot)^\dagger$ stand for the conjugate, transpose, conjugate transpose and pseudo-inverse operators, respectively. $\mathbb{E}$ denotes the expectation, $\mathbf{B}^{(-k)}$ is the result of removing the kth column of $\mathbf{B}$, and $diag\{a_1, a_2, \cdots, a_M\}$ is the diagonal matrix with $a_1, a_2, \cdots, a_M$ being its diagonal elements. $\mathbf{j} = \sqrt{-1}$ and $|x|$ is the magnitude of x. $\lfloor \cdot \rfloor$ and $\lceil \cdot \rceil$ denote the integer floor and ceiling operators, respectively, and $\mathbf{vec}\{\mathbf{X}\}$ defines the column stacking operator, which stacks the columns of $\mathbf{X}$ into a vector, while $\mathbf{\Pi}_M$ is the $M \times M$ exchange matrix with ones on its anti-diagonal elements and zeros elsewhere. Finally, $\text{tr}(\cdot)$ denotes the matrix trace operator.

II. SYSTEM MODEL

We assume that K uncorrelated narrowband and CD source signals transmitted by the K user terminals impinge on the
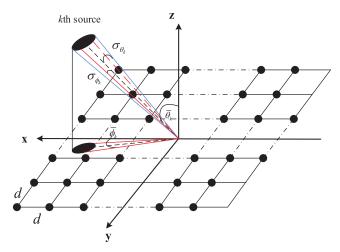

FIGURE 1. Illustration of a coherently distributed source impinging on a URA.

URA of the BS. The URA is composed of a grid of M azimuth antenna elements and N elevation antenna elements with an element spacing of d. Fig. 1 illustrates the kth CD source that impinges on the URA, where $\bar{\phi}_k$ and $\bar{\theta}_k$ are the central azimuth and elevation DOAs of the kth source, while σ_{ϕ_k} and σ_{θ_k} are the kth source's azimuth and elevation angular spreads, respectively. A distributed source is the superposition of all contributors, i.e., it consists of many 'point' sources distributed or spread over some angular volume. Hence, the kth CD source can be modeled by a stochastic process, where the azimuth and elevation DOAs (ϕ_k, θ_k) obey a random angular distribution with the central DOAs $(\bar{\phi}_k, \bar{\theta}_k)$ and the angular spreads $(\sigma_{\phi_k}, \sigma_{\theta_k})$. The parameters of the angular distribution for the kth source are therefore given by

$$\boldsymbol{\mu}_k = \begin{bmatrix} \bar{\phi}_k \ \bar{\theta}_k \ \sigma_{\phi_k} \ \sigma_{\theta_k} \end{bmatrix}^T. \quad (1)$$

Generally, $0° \leq \bar{\phi}_k \leq 180°$ and $0° \leq \bar{\theta}_k \leq 90°$ [19], while σ_{θ_k} and σ_{ϕ_k} are sufficiently small. Employing the center of the URA as the phase reference, the responses or steering vectors for the DOAs (ϕ_k, θ_k) can be denoted by $\mathbf{a}(\phi_k, \theta_k) \in \mathbb{C}^{MN \times 1}$, whose ith element is given by [38]

$$\left[\mathbf{a}(\phi_k, \theta_k)\right]_i = e^{\mathbf{j}\left(\left(m - \frac{M+1}{2}\right)u_k + \left(n - \frac{N+1}{2}\right)v_k\right)},$$
$$\text{for } i = (m-1)N + n, \ 1 \leq m \leq M, \ 1 \leq n \leq N, \quad (2)$$

with

$$v_k = \frac{2\pi d}{\lambda} \sin \phi_k \sin \theta_k, \quad (3)$$

$$u_k = \frac{2\pi d}{\lambda} \cos \phi_k \sin \theta_k, \quad (4)$$

where λ is the carrier's wavelength. The kth signal received by the URA can be expressed as [22]

$$\mathbf{s}_k(t) = \int \int \mathbf{a}(\phi_k, \theta_k) \varsigma_k(t, \phi_k, \theta_k; \boldsymbol{\mu}_k) d\phi_k d\theta_k, \quad (5)$$

where $t \in \{1, 2, \cdots, T\}$ with T being the number of temporal received signal samples, and the integration range spreads

over the angular volume of (ϕ_k, θ_k), while the angular signal intensity $\varsigma_k(t, \phi_k, \theta_k; \boldsymbol{\mu}_k)$ can be represented by

$$\varsigma_k(t, \phi_k, \theta_k; \boldsymbol{\mu}_k) = \bar{s}_k(t)\rho(\phi_k, \theta_k; \boldsymbol{\mu}_k), \quad (6)$$

in which $\bar{s}_k(t)$ denotes the complex temporal envelope of the kth source with the transmitted power $\mathbb{E}\{|\bar{s}_k(t)|^2\} = P_k$, and the underlying angular density of the kth user, $\rho(\phi_k, \theta_k; \boldsymbol{\mu}_k)$, follows the Gaussian distribution [21], [34]

$$\rho(\phi_k, \theta_k; \boldsymbol{\mu}_k) = \frac{1}{2\pi \sigma_{\phi_k} \sigma_{\theta_k}} e^{-\frac{1}{2}\left(\frac{(\phi_k - \bar{\phi}_k)^2}{\sigma_{\phi_k}^2} + \frac{(\theta_k - \bar{\theta}_k)^2}{\sigma_{\theta_k}^2}\right)}. \quad (7)$$

The output vector of the URA at temporal sample t, $\mathbf{x}(t) \in \mathbb{C}^{MN \times 1}$, is then given by

$$\mathbf{x}(t) = \sum_{k=1}^{K} \mathbf{s}_k(t) + \mathbf{n}(t), \quad (8)$$

where $\mathbf{n}(t)$ is the white sensor noise vector with zero mean and covariance matrix $\mathbb{E}\{\mathbf{n}(t)\mathbf{n}^H(t)\} = \sigma_n^2 \mathbf{I}_{MN}$.

Define the generalized steering vector for user k as

$$\mathbf{b}(\boldsymbol{\mu}_k) = \iint \mathbf{a}(\phi_k, \theta_k)\rho(\phi_k, \theta_k; \boldsymbol{\mu}_k) d\phi_k d\theta_k \in \mathbb{C}^{MN \times 1}. \quad (9)$$

By denoting $\mathbf{B} = [\mathbf{b}(\boldsymbol{\mu}_1)\, \mathbf{b}(\boldsymbol{\mu}_2) \cdots \mathbf{b}(\boldsymbol{\mu}_K)] \in \mathbb{C}^{MN \times K}$ and $\bar{\mathbf{s}}(t) = [\bar{s}_1(t)\, \bar{s}_2(t) \cdots \bar{s}_K(t)]^T \in \mathbb{C}^{K \times 1}$, we can express (8) as

$$\mathbf{x}(t) = \mathbf{B}\bar{\mathbf{s}}(t) + \mathbf{n}(t). \quad (10)$$

The azimuth and elevation DOAs can be expressed as $\phi_k = \bar{\phi}_k + \tilde{\phi}_k$ and $\theta_k = \bar{\theta}_k + \tilde{\theta}_k$ [19], where $\bar{\phi}_k$ and $\bar{\theta}_k$ are the means of ϕ_k and θ_k, respectively, while $\tilde{\phi}_k$ and $\tilde{\theta}_k$ are the corresponding random angular deviations with zero mean and standard deviations σ_{ϕ_k} and σ_{θ_k}, respectively. Since $\tilde{\phi}_k$ and $\tilde{\theta}_k$ are sufficiently small, we have $\sin \tilde{\phi}_k \approx \tilde{\phi}_k$, $\sin \tilde{\theta}_k \approx \tilde{\theta}_k$, $\cos \tilde{\phi}_k \approx 1$, $\cos \tilde{\theta}_k \approx 1$ and $\tilde{\theta}_k \tilde{\phi}_k \approx 0$. Further define

$$\underline{c}_k^i = \left(m - \frac{M+1}{2}\right) \sin \bar{\phi}_k \sin \bar{\theta}_k, \quad (11)$$

$$\underline{l}_k^i = \left(n - \frac{N+1}{2}\right) \cos \bar{\phi}_k \sin \bar{\theta}_k, \quad (12)$$

$$\underline{g}_k^i = \left(m - \frac{M+1}{2}\right) \cos \bar{\phi}_k \cos \bar{\theta}_k, \quad (13)$$

$$\underline{o}_k^i = \left(n - \frac{N+1}{2}\right) \sin \bar{\phi}_k \cos \bar{\theta}_k. \quad (14)$$

Then, the ith element of $\mathbf{b}(\boldsymbol{\mu}_k)$ is given in (15) at the bottom of this page. With the aid of integral formula [39]

$$\int_{-\infty}^{\infty} e^{-f^2 x^2} e^{\mathbf{j}p(x+\alpha)} dx = \frac{\sqrt{\pi}}{f} e^{-\frac{p^2}{4f^2}} e^{\mathbf{j}p\alpha}, \quad (16)$$

(15) can be expressed as

$$[\mathbf{b}(\boldsymbol{\mu}_k)]_i \approx [\mathbf{a}(\bar{\phi}_k, \bar{\theta}_k)]_i \cdot [\mathbf{h}(\boldsymbol{\mu}_k)]_i, \quad (17)$$

where

$$[\mathbf{h}(\boldsymbol{\mu}_k)]_i = e^{-\frac{2\pi^2 d^2 \sigma_{\phi_k}^2}{\lambda^2}(-\underline{c}_k + \underline{l}_k)^2} e^{-\frac{2\pi^2 d^2 \sigma_{\theta_k}^2}{\lambda^2}(\underline{g}_k + \underline{o}_k)^2}$$

$$= e^{-\frac{2\pi^2 d^2 \sigma_{\phi_k}^2}{\lambda^2}(\underline{c}_k^2 + \underline{l}_k^2)} e^{-\frac{2\pi^2 d^2 \sigma_{\theta_k}^2}{\lambda^2}(\underline{g}_k^2 + \underline{o}_k^2)}$$

$$\cdot e^{\frac{2\pi^2 d^2 \sigma_{\phi_k}^2}{\lambda^2} 2\underline{c}_k \underline{l}_k} e^{-\frac{2\pi^2 d^2 \sigma_{\theta_k}^2}{\lambda^2} 2\underline{g}_k \underline{o}_k}. \quad (18)$$

Since $\sigma_{\theta_k}^2$ and $\sigma_{\phi_k}^2$ are sufficiently small, all four terms of $[\mathbf{h}(\boldsymbol{\mu}_k)]_i$ given in (18) are very close to 1. Using the simple inequality $x^2 + y^2 > \pm 2xy$, we can infer that the third and fourth terms are closer to 1 than the first and second terms. Therefore, we may approximate $[\mathbf{h}(\boldsymbol{\mu}_k)]_i$ by the first and second terms, namely,

$$[\mathbf{h}(\boldsymbol{\mu}_k)]_i \approx e^{-\frac{2\pi^2 d^2 \sigma_{\phi_k}^2}{\lambda^2}(\underline{c}_k^2 + \underline{l}_k^2)} e^{-\frac{2\pi^2 d^2 \sigma_{\theta_k}^2}{\lambda^2}(\underline{g}_k^2 + \underline{o}_k^2)}. \quad (19)$$

Similar to the definition of $\mathbf{a}(\phi_k, \theta_k)$, we define the azimuth and elevation subarrays' steering vectors as $\mathbf{a}_x(\phi_k, \theta_k)_n \in \mathbb{C}^{M \times 1}$ for $1 \leq n \leq N$ and $\mathbf{a}_y(\phi_k, \theta_k)_m \in \mathbb{C}^{N \times 1}$ for $1 \leq m \leq M$, respectively. The mth element of $\mathbf{a}_x(\phi_k, \theta_k)_n$ and the nth element of $\mathbf{a}_y(\phi_k, \theta_k)_m$ are given by

$$[\mathbf{a}_x(\phi_k, \theta_k)_n]_m = [\mathbf{a}_y(\phi_k, \theta_k)_m]_n = [\mathbf{a}(\phi_k, \theta_k)]_i$$

$$= e^{-\mathbf{j}\left(\left(m - \frac{M+1}{2}\right)u_k + \left(n - \frac{N+1}{2}\right)v_k\right)},$$

$$i = (m-1)N + n, \ 1 \leq m \leq M, \ 1 \leq n \leq N. \quad (20)$$

Then, the nth and mth generalized steering vectors of the azimuth and elevation directions can be defined as

$$\mathbf{b}_x(\boldsymbol{\mu}_k)_n = \iint \mathbf{a}_x(\phi_k, \theta_k)_n \rho(\phi_k, \theta_k; \boldsymbol{\mu}_k) d\phi_k d\theta_k, \quad (21)$$

$$\mathbf{b}_y(\boldsymbol{\mu}_k)_m = \iint \mathbf{a}_y(\phi_k, \theta_k)_m \rho(\phi_k, \theta_k; \boldsymbol{\mu}_k) d\phi_k d\theta_k. \quad (22)$$

$$[\mathbf{b}(\boldsymbol{\mu}_k)]_i = \iint \frac{[\mathbf{a}(\phi_k, \theta_k)]_i}{2\pi \sigma_{\phi_k} \sigma_{\theta_k}} e^{-\frac{1}{2}\left(\frac{(\phi_k - \bar{\phi}_k)^2}{\sigma_{\phi_k}^2} + \frac{(\theta_k - \bar{\theta}_k)^2}{\sigma_{\theta_k}^2}\right)} d\phi_k d\theta_k$$

$$= \frac{1}{2\pi \sigma_{\phi_k} \sigma_{\theta_k}} \iint e^{\mathbf{j}\frac{2\pi d}{\lambda}\left(\left(m - \frac{M+1}{2}\right)\cos\phi_k \sin\theta_k + \left(n - \frac{N+1}{2}\right)\sin\phi_k \sin\theta_k\right)} e^{-\frac{1}{2}\left(\frac{(\phi_k - \bar{\phi}_k)^2}{\sigma_{\phi_k}^2} + \frac{(\theta_k - \bar{\theta}_k)^2}{\sigma_{\theta_k}^2}\right)} d\phi_k d\theta_k$$

$$\approx \frac{1}{2\pi \sigma_{\phi_k} \sigma_{\theta_k}} [\mathbf{a}(\bar{\phi}_k, \bar{\theta}_k)]_i \int e^{\mathbf{j}\frac{2\pi d}{\lambda}\tilde{\phi}_k(-\underline{c}_k + \underline{l}_k)} e^{-\frac{\tilde{\phi}_k^2}{2\sigma_{\phi_k}^2}} d\tilde{\phi}_k \int e^{\mathbf{j}\frac{2\pi d}{\lambda}\tilde{\theta}_k(\underline{g}_k + \underline{o}_k)} e^{-\frac{\tilde{\theta}_k^2}{2\sigma_{\theta_k}^2}} d\tilde{\theta}_k. \quad (15)$$

Following the same procedure for deriving (17) and (19), it can be shown that the responses of the central subarrays in the azimuth and elevation directions can be expressed as

$$\left[\mathbf{b}_x(\boldsymbol{\mu}_k)_{\frac{N+1}{2}}\right]_m \approx \left[\mathbf{a}_x(\bar{\phi}_k, \bar{\theta}_k)_{\frac{N+1}{2}}\right]_m \cdot \left[\mathbf{h}_x(\boldsymbol{\mu}_k)_{\frac{N+1}{2}}\right]_m, \quad (23)$$

$$\left[\mathbf{b}_y(\boldsymbol{\mu}_k)_{\frac{M+1}{2}}\right]_n \approx \left[\mathbf{a}_y(\bar{\phi}_k, \bar{\theta}_k)_{\frac{M+1}{2}}\right]_n \cdot \left[\mathbf{h}_y(\boldsymbol{\mu}_k)_{\frac{M+1}{2}}\right]_n, \quad (24)$$

with

$$\left[\mathbf{h}_x(\boldsymbol{\mu}_k)_{\frac{N+1}{2}}\right]_m \approx e^{-\frac{2\pi^2 \, d^2 \sigma_{\phi_k}^2}{\lambda^2} \underline{c}_k^2} e^{-\frac{2\pi^2 \, d^2 \sigma_{\theta_k}^2}{\lambda^2} \underline{g}_k^2}, \quad (25)$$

$$\left[\mathbf{h}_y(\boldsymbol{\mu}_k)_{\frac{M+1}{2}}\right]_n \approx e^{-\frac{2\pi^2 d^2 \sigma_{\phi_k}^2}{\lambda^2} l_k^2} e^{-\frac{2\pi^2 d^2 \sigma_{\theta_k}^2}{\lambda^2} o_k^2}. \quad (26)$$

Note that for odd M and N, (23) and (24) represent the responses of the central azimuth and elevation subarrays. For even M and N, however, they represent the responses of the virtual central azimuth and elevation subarrays, since such central azimuth and elevation subarrays do not physically exist. Since $[\mathbf{a}(\bar{\phi}_k, \bar{\theta}_k)]_i = \left[\mathbf{a}_x(\bar{\phi}_k, \bar{\theta}_k)_{\frac{N+1}{2}}\right]_m \cdot \left[\mathbf{a}_y(\bar{\phi}_k, \bar{\theta}_k)_{\frac{M+1}{2}}\right]_n$ and $[\mathbf{h}(\boldsymbol{\mu}_k)]_i = \left[\mathbf{h}_x(\boldsymbol{\mu}_k)_{\frac{N+1}{2}}\right]_m \cdot \left[\mathbf{h}_y(\boldsymbol{\mu}_k)_{\frac{M+1}{2}}\right]_n$, we have

$$[\mathbf{b}(\boldsymbol{\mu}_k)]_i \approx \left[\mathbf{b}_x(\boldsymbol{\mu}_k)_{\frac{N+1}{2}}\right]_m \cdot \left[\mathbf{b}_y(\boldsymbol{\mu}_k)_{\frac{M+1}{2}}\right]_n. \quad (27)$$

Consequently, the generalized steering vector $\mathbf{b}(\boldsymbol{\mu}_k)$ has the following approximate Kronecker product decomposition

$$\mathbf{b}(\boldsymbol{\mu}_k) \approx \mathbf{b}_x(\boldsymbol{\mu}_k)_{\frac{N+1}{2}} \otimes \mathbf{b}_y(\boldsymbol{\mu}_k)_{\frac{M+1}{2}}. \quad (28)$$

III. THE 2D UNITARY ESPRIT-BASED ALGORITHM

This section details our proposed joint angle estimation and signal reconstruction techniques conceived for 2D CD sources in massive MIMO systems employing URA. We first prove the approximate rotational invariance property of the subarray's response in both the azimuth and elevation directions. By exploiting this rotational invariance structure, we propose the 2D unitary ESPRIT-based algorithm for estimating the 2D central DOAs of CD sources. We further propose a closed-form estimator for the angular spreads, which completely avoids the high-complexity spectrum peak searching and paring process. Finally, signal reconstruction is considered.

A. APPROXIMATE ROTATIONAL INVARIANCE

Theorem 1: The subarrays in both the azimuth and elevation directions are approximately rotationally invariant. More specifically, the elements of $\mathbf{b}_x(\boldsymbol{\mu}_k)_n$ have the same magnitude

$$\left|\left[\mathbf{b}_x(\boldsymbol{\mu}_k)_n\right]_p\right| = \left|\left[\mathbf{b}_x(\boldsymbol{\mu}_k)_n\right]_q\right|, \quad (29)$$

and the elements of $\mathbf{b}_y(\boldsymbol{\mu}_k)_m$ have the same magnitude

$$\left|\left[\mathbf{b}_y(\boldsymbol{\mu}_k)_m\right]_p\right| = \left|\left[\mathbf{b}_y(\boldsymbol{\mu}_k)_m\right]_q\right|. \quad (30)$$
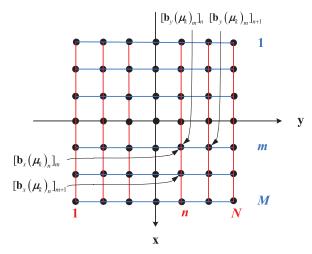

FIGURE 2. Illustration of the azimuth and elevation subarrays of URA.

Proof: Refer to Fig. 2 and consider $\left[\mathbf{b}_x(\boldsymbol{\mu}_k)_n\right]_{m+1}$ for $1 \le n \le N$ and $1 \le m \le M - 1$. According to the definition of the subarray's generalized steering vector, we have

$$\left[\mathbf{b}_x(\boldsymbol{\mu}_k)_n\right]_{m+1} = \iint [\mathbf{a}_x(\phi_k, \theta_k)_n]_{m+1} \rho(\phi_k, \theta_k; \boldsymbol{\mu}_k) \, d\phi_k d\theta_k$$
$$= \iint [\mathbf{a}_x(\phi_k, \theta_k)_n]_m e^{j u_k} \rho(\phi_k, \theta_k; \boldsymbol{\mu}_k) \, d\phi_k d\theta_k. \quad (31)$$

Similar to the derivation of (15), we can show that

$$\left[\mathbf{b}_x(\boldsymbol{\mu}_k)_n\right]_{m+1}$$
$$\approx \frac{e^{j\bar{u}_k}}{2\pi \sigma_{\phi_k} \sigma_{\theta_k}} [\mathbf{a}(\bar{\phi}_k, \bar{\theta}_k)]_i$$
$$\cdot \int e^{j\frac{2\pi d}{\lambda} \widetilde{\phi}_k \left(-\underline{c}_k + l_k\right)} e^{-\frac{\widetilde{\phi}_k^2}{2\sigma_{\phi_k}^2}} d\widetilde{\phi}_k \int e^{j\frac{2\pi d}{\lambda} \widetilde{\theta}_k \left(\underline{g}_k + o_k\right)} e^{-\frac{\widetilde{\theta}_k^2}{2\sigma_{\theta_k}^2}} d\widetilde{\theta}_k$$
$$\approx e^{j\bar{u}_k} \left[\mathbf{b}(\boldsymbol{\mu}_k)\right]_i, \quad (32)$$

where

$$\bar{u}_k = \frac{2\pi d}{\lambda} \cos\bar{\phi}_k \sin\bar{\theta}_k. \quad (33)$$

Since $\left[\mathbf{a}(\phi_k, \theta_k)\right]_i = \left[\mathbf{a}_x(\phi_k, \theta_k)_n\right]_m$, from (15), it is clear that $\left[\mathbf{b}(\boldsymbol{\mu}_k)\right]_i = \left[\mathbf{b}_x(\boldsymbol{\mu}_k)_n\right]_m$. Hence, we arrive at

$$\left[\mathbf{b}_x(\boldsymbol{\mu}_k)_n\right]_{m+1} \approx e^{j\bar{u}_k} \left[\mathbf{b}_x(\boldsymbol{\mu}_k)_n\right]_m. \quad (34)$$

In a similar way, we have

$$\left[\mathbf{b}_y(\boldsymbol{\mu}_k)_m\right]_{n+1} \approx e^{j\bar{v}_k} \left[\mathbf{b}_y(\boldsymbol{\mu}_k)_m\right]_n, \quad (35)$$

where

$$\bar{v}_k = \frac{2\pi d}{\lambda} \sin\bar{\phi}_k \sin\bar{\theta}_k. \quad (36)$$

This completes the proof. ∎

According to Theorem 1, we have

$$e^{j\bar{u}_k}(\mathbf{J}_1 \otimes \mathbf{I}_N)\mathbf{b}(\boldsymbol{\mu}_k) = (\mathbf{J}_2 \otimes \mathbf{I}_N)\mathbf{b}(\boldsymbol{\mu}_k), \quad (37)$$

$$e^{j\bar{v}_k}(\mathbf{I}_M \otimes \mathbf{J}_3)\mathbf{b}(\boldsymbol{\mu}_k) = (\mathbf{I}_M \otimes \mathbf{J}_4)\mathbf{b}(\boldsymbol{\mu}_k), \quad (38)$$

where $\mathbf{J}_1$ and $\mathbf{J}_2$ are the $(M-1) \times M$ selection matrices defined respectively by

$$\mathbf{J}_1 = \begin{bmatrix} \mathbf{I}_{M-1} & \mathbf{0} \end{bmatrix} \in \mathbb{R}^{(M-1) \times M}, \tag{39}$$

$$\mathbf{J}_2 = \begin{bmatrix} \mathbf{0} & \mathbf{I}_{M-1} \end{bmatrix} \in \mathbb{R}^{(M-1) \times M}, \tag{40}$$

while $\mathbf{J}_3$ and $\mathbf{J}_4$ are the $(N-1) \times N$ selection matrices defined respectively by

$$\mathbf{J}_3 = \begin{bmatrix} \mathbf{I}_{N-1} & \mathbf{0} \end{bmatrix} \in \mathbb{R}^{(N-1) \times N}, \tag{41}$$

$$\mathbf{J}_4 = \begin{bmatrix} \mathbf{0} & \mathbf{I}_{N-1} \end{bmatrix} \in \mathbb{R}^{(N-1) \times N}. \tag{42}$$

B. 2D UNITARY ESPRIT-BASED DOA ESTIMATION

Employing the center of the URA as the phase reference, the array manifolds of $\mathbf{a}_x(\bar{\phi}_k, \bar{\theta}_k)_{\frac{N+1}{2}}$ and $\mathbf{a}_y(\bar{\phi}_k, \bar{\theta}_k)_{\frac{M+1}{2}}$ are conjugate centrosymmetric [38]. In fact, from (20), it can readily be seen that $\mathbf{\Pi}_M \mathbf{a}_x(\bar{\phi}_k, \bar{\theta}_k)_{\frac{N+1}{2}} = \mathbf{a}_x^*(\bar{\phi}_k, \bar{\theta}_k)_{\frac{N+1}{2}}$ and $\mathbf{\Pi}_N \mathbf{a}_y(\bar{\phi}_k, \bar{\theta}_k)_{\frac{M+1}{2}} = \mathbf{a}_y^*(\bar{\phi}_k, \bar{\theta}_k)_{\frac{M+1}{2}}$. Similarly, from (25) and (26) as well as (11) to (14), we can see that the real-valued $\mathbf{h}_x(\boldsymbol{\mu}_k)_{\frac{N+1}{2}}$ and $\mathbf{h}_y(\boldsymbol{\mu}_k)_{\frac{M+1}{2}}$ are centrosymmetric. Then, following from (23) and (24), $\mathbf{b}_x(\boldsymbol{\mu}_k)_{\frac{N+1}{2}}$ and $\mathbf{b}_y(\boldsymbol{\mu}_k)_{\frac{M+1}{2}}$ are approximately conjugate centrosymmetric.

Since the inner product of two conjugate centrosymmetric vectors is real-valued, any matrix whose rows are conjugate centrosymmetric can be applied to transform the complex-valued manifolds $\mathbf{b}_x(\boldsymbol{\mu}_k)_{\frac{N+1}{2}}$ and $\mathbf{b}_y(\boldsymbol{\mu}_k)_{\frac{M+1}{2}}$ into real-valued manifolds. Taking $\mathbf{b}_x(\boldsymbol{\mu}_k)_{\frac{N+1}{2}}$ as an example and assuming an odd M, the simplest matrix achieving this goal can be constructed as

$$\mathbf{Q}_M = \frac{1}{\sqrt{2}} \begin{bmatrix} \mathbf{I}_{\lceil \frac{M-1}{2} \rceil} & \mathbf{0} & j\mathbf{I}_{\lceil \frac{M-1}{2} \rceil} \\ \mathbf{0}^T & \sqrt{2} & \mathbf{0}^T \\ \mathbf{\Pi}_{\lceil \frac{M-1}{2} \rceil} & \mathbf{0} & -j\mathbf{\Pi}_{\lceil \frac{M-1}{2} \rceil} \end{bmatrix}. \tag{43}$$

By contrast, if M is even, an appropriate unitary matrix is obtained from (43) by removing its center row and center column, which is still denoted as $\mathbf{Q}_M$ for notational convenience. We can see that $\mathbf{Q}_M$ is a sparse unitary matrix that transforms $\mathbf{b}_x(\boldsymbol{\mu}_k)_{\frac{N+1}{2}}$ into an $M \times 1$ real-valued manifold

$$\mathbf{d}_x(\boldsymbol{\mu}_k)_{\frac{N+1}{2}} = \mathbf{Q}_M^H \mathbf{b}_x(\boldsymbol{\mu}_k)_{\frac{N+1}{2}}. \tag{44}$$

Similarly, we can construct the sparse unitary matrix $\mathbf{Q}_N$ that transforms $\mathbf{b}_y(\boldsymbol{\mu}_k)_{\frac{M+1}{2}}$ into a real-valued one

$$\mathbf{d}_y(\boldsymbol{\mu}_k)_{\frac{M+1}{2}} = \mathbf{Q}_N^H \mathbf{b}_y(\boldsymbol{\mu}_k)_{\frac{M+1}{2}}. \tag{45}$$

Pre-multiplying $\mathbf{b}(\boldsymbol{\mu}_k)$ by $\mathbf{Q}_M^H \otimes \mathbf{Q}_N^H$ creates the real-valued manifold

$$\begin{aligned} \mathbf{d}(\boldsymbol{\mu}_k) &= (\mathbf{Q}_M^H \otimes \mathbf{Q}_N^H) \mathbf{b}(\boldsymbol{\mu}_k) \\ &\approx (\mathbf{Q}_M^H \otimes \mathbf{Q}_N^H)(\mathbf{b}_x(\boldsymbol{\mu}_k)_{\frac{N+1}{2}} \otimes \mathbf{b}_y(\boldsymbol{\mu}_k)_{\frac{M+1}{2}}) \\ &= (\mathbf{Q}_M^H \mathbf{b}_x(\boldsymbol{\mu}_k)_{\frac{N+1}{2}}) \otimes (\mathbf{Q}_N^H \mathbf{b}_y(\boldsymbol{\mu}_k)_{\frac{M+1}{2}}) \\ &= \mathbf{d}_x(\boldsymbol{\mu}_k)_{\frac{N+1}{2}} \otimes \mathbf{d}_y(\boldsymbol{\mu}_k)_{\frac{M+1}{2}}. \end{aligned} \tag{46}$$

Since $\mathbf{Q}_M$ and $\mathbf{Q}_N$ are unitary matrices, (37) can be rewritten as

$$\begin{aligned} e^{j\bar{u}_k} &(\mathbf{J}_1 \otimes \mathbf{I}_N)(\mathbf{Q}_M \otimes \mathbf{Q}_N)(\mathbf{Q}_M^H \otimes \mathbf{Q}_N^H) \mathbf{b}(\boldsymbol{\mu}_k) \\ &= (\mathbf{J}_2 \otimes \mathbf{I}_N)(\mathbf{Q}_M \otimes \mathbf{Q}_N)(\mathbf{Q}_M^H \otimes \mathbf{Q}_N^H) \mathbf{b}(\boldsymbol{\mu}_k). \end{aligned} \tag{47}$$

Pre-multiplying both sides of (47) by $\mathbf{Q}_{M-1}^H \otimes \mathbf{Q}_N^H$ and noting (46) yields the following invariance relationship

$$\begin{aligned} e^{j\bar{u}_k} &(\mathbf{Q}_{M-1}^H \otimes \mathbf{Q}_N^H)(\mathbf{J}_1 \otimes \mathbf{I}_N)(\mathbf{Q}_M \otimes \mathbf{Q}_N) \mathbf{d}(\boldsymbol{\mu}_k) \\ &= (\mathbf{Q}_{M-1}^H \otimes \mathbf{Q}_N^H)(\mathbf{J}_2 \otimes \mathbf{I}_N)(\mathbf{Q}_M \otimes \mathbf{Q}_N) \mathbf{d}(\boldsymbol{\mu}_k). \end{aligned} \tag{48}$$

That is,

$$\begin{aligned} e^{j\bar{u}_k} &\left((\mathbf{Q}_{M-1}^H \mathbf{J}_1 \mathbf{Q}_M) \otimes \mathbf{I}_N\right) \mathbf{d}(\boldsymbol{\mu}_k) \\ &= \left((\mathbf{Q}_{M-1}^H \mathbf{J}_2 \mathbf{Q}_M) \otimes \mathbf{I}_N\right) \mathbf{d}(\boldsymbol{\mu}_k). \end{aligned} \tag{49}$$

Noting that $\mathbf{J}_1$ and $\mathbf{J}_2$ satisfy $\mathbf{\Pi}_{M-1} \mathbf{J}_2 \mathbf{\Pi}_M = \mathbf{J}_1$, as well as $\mathbf{\Pi}_M \mathbf{Q}_M = \mathbf{Q}_M^*$ and $\mathbf{\Pi}_M \mathbf{\Pi}_M = \mathbf{I}_M$, we have

$$\begin{aligned} \mathbf{Q}_{M-1}^H \mathbf{J}_2 \mathbf{Q}_M &= \mathbf{Q}_{M-1}^H \mathbf{\Pi}_{M-1} \mathbf{\Pi}_{M-1} \mathbf{J}_2 \mathbf{\Pi}_M \mathbf{\Pi}_M \mathbf{Q}_M \\ &= \mathbf{Q}_{M-1}^T \mathbf{J}_1 \mathbf{Q}_M^* = (\mathbf{Q}_{M-1}^H \mathbf{J}_1 \mathbf{Q}_M)^*. \end{aligned} \tag{50}$$

Let the real-valued $(M-1) \times M$ matrices $\mathbf{K}_1$ and $\mathbf{K}_2$ be the real and imaginary parts of $\mathbf{Q}_{M-1}^H \mathbf{J}_2 \mathbf{Q}_M$, respectively, i.e.,

$$\mathbf{K}_1 = \Re\{\mathbf{Q}_{M-1}^H \mathbf{J}_2 \mathbf{Q}_M\}, \tag{51}$$

$$\mathbf{K}_2 = \Im\{\mathbf{Q}_{M-1}^H \mathbf{J}_2 \mathbf{Q}_M\}. \tag{52}$$

Further define

$$\mathbf{K}_{u_1} = \mathbf{K}_1 \otimes \mathbf{I}_N, \tag{53}$$

$$\mathbf{K}_{u_2} = \mathbf{K}_2 \otimes \mathbf{I}_N. \tag{54}$$

Then, the invariance relationship (49) can be rewritten as

$$e^{j\frac{\bar{u}_k}{2}}(\mathbf{K}_{u_1} - j\mathbf{K}_{u_2}) \mathbf{d}(\boldsymbol{\mu}_k) = e^{-j\frac{\bar{u}_k}{2}}(\mathbf{K}_{u_1} + j\mathbf{K}_{u_2}) \mathbf{d}(\boldsymbol{\mu}_k). \tag{55}$$

In other words, this invariance relationship only involves real-valued quantities, and it can be expressed as

$$\tan\left(\frac{\bar{u}_k}{2}\right) \mathbf{K}_{u_1} \mathbf{d}(\boldsymbol{\mu}_k) = \mathbf{K}_{u_2} \mathbf{d}(\boldsymbol{\mu}_k). \tag{56}$$

Similarly, from (38), we have the invariance relationship

$$\begin{aligned} e^{j\bar{v}_k} &\left(\mathbf{I}_M \otimes (\mathbf{Q}_{N-1}^H \mathbf{J}_3 \mathbf{Q}_N)\right) \mathbf{d}(\boldsymbol{\mu}_k) \\ &= \left(\mathbf{I}_M \otimes (\mathbf{Q}_{N-1}^H \mathbf{J}_4 \mathbf{Q}_N)\right) \mathbf{d}(\boldsymbol{\mu}_k). \end{aligned} \tag{57}$$

Let $\mathbf{K}_3$ and $\mathbf{K}_4$ be

$$\mathbf{K}_3 = \Re\{\mathbf{Q}_{N-1}^H \mathbf{J}_4 \mathbf{Q}_N\}, \tag{58}$$

$$\mathbf{K}_4 = \Im\{\mathbf{Q}_{N-1}^H \mathbf{J}_4 \mathbf{Q}_N\}, \tag{59}$$

and further define

$$\mathbf{K}_{v_1} = \mathbf{I}_M \otimes \mathbf{K}_3, \tag{60}$$

$$\mathbf{K}_{v_2} = \mathbf{I}_M \otimes \mathbf{K}_4. \tag{61}$$

Then, the invariance relationship (57) only involves real-valued quantities, and it can be expressed as

$$\tan\left(\frac{\bar{v}_k}{2}\right)\mathbf{K}_{v_1}\mathbf{d}(\boldsymbol{\mu}_k) = \mathbf{K}_{v_2}\mathbf{d}(\boldsymbol{\mu}_k). \tag{62}$$

Consider the DOA matrix $\mathbf{D} = [\mathbf{d}(\boldsymbol{\mu}_1)\,\mathbf{d}(\boldsymbol{\mu}_2)\cdots\mathbf{d}(\boldsymbol{\mu}_K)]$ $\in \mathbb{R}^{MN \times K}$. From (56) and (62), $\mathbf{D}$ satisfies

$$\mathbf{K}_{u_1}\mathbf{D}\boldsymbol{\Omega}_u = \mathbf{K}_{u_2}\mathbf{D}, \tag{63}$$

$$\mathbf{K}_{v_1}\mathbf{D}\boldsymbol{\Omega}_v = \mathbf{K}_{v_2}\mathbf{D}, \tag{64}$$

where

$$\boldsymbol{\Omega}_u = diag\left\{\tan\left(\frac{\bar{u}_1}{2}\right), \tan\left(\frac{\bar{u}_2}{2}\right), \cdots, \tan\left(\frac{\bar{u}_K}{2}\right)\right\}, \tag{65}$$

$$\boldsymbol{\Omega}_v = diag\left\{\tan\left(\frac{\bar{v}_1}{2}\right), \tan\left(\frac{\bar{v}_2}{2}\right), \cdots, \tan\left(\frac{\bar{v}_K}{2}\right)\right\}. \tag{66}$$

It is worth noting again that after the unitary transformation, all the matrices involved are real-valued, which significantly reduces the computational complexity.

Let $\mathbf{X} = [\mathbf{x}(1)\,\mathbf{x}(2)\cdots\mathbf{x}(T)] \in \mathbb{C}^{MN \times T}$ be the complex-valued data matrix containing T snapshots as columns. As discussed in [38], the approximate signal eigenvectors for the unitary ESPRIT, collected together as $\mathbf{E}_\Lambda$, are associated with the K largest singular values of the real-valued matrix $\mathbf{\Lambda} = [\Re\{\mathbf{Y}\}\,\Im\{\mathbf{Y}\}]$, where $\mathbf{Y} = (\mathbf{Q}_M^H \otimes \mathbf{Q}_N^H)\mathbf{X}$. In particular, as the number of snapshots $T \to \infty$, the subspace spanned by the columns of the $MN \times K$ real-valued matrix $\mathbf{E}_\Lambda$ becomes the same subspace spanned by the columns of the $MN \times K$ real-valued steering matrix $\mathbf{D}$. Therefore, we have $\mathbf{E}_\Lambda = \mathbf{DT}$ in which $\mathbf{T}$ is an unknown $K \times K$ full-rank real-valued matrix. Substituting $\mathbf{D} = \mathbf{E}_\Lambda\mathbf{T}^{-1}$ into (63) and (64) yields

$$\mathbf{K}_{u_1}\mathbf{E}_\Lambda\boldsymbol{\Psi}_u = \mathbf{K}_{u_2}\mathbf{E}_\Lambda \text{ with } \boldsymbol{\Psi}_u = \mathbf{T}^{-1}\boldsymbol{\Omega}_u\mathbf{T}, \tag{67}$$

$$\mathbf{K}_{v_1}\mathbf{E}_\Lambda\boldsymbol{\Psi}_v = \mathbf{K}_{v_2}\mathbf{E}_\Lambda \text{ with } \boldsymbol{\Psi}_v = \mathbf{T}^{-1}\boldsymbol{\Omega}_v\mathbf{T}. \tag{68}$$

$\boldsymbol{\Psi}_u$ and $\boldsymbol{\Psi}_v$ in (67) and (68) are solved by the LS or total LS algorithm. Automatic pairing of the $\bar{u}_k$ and $\bar{v}_k$ spatial frequency estimates can be used because all of the quantities in (67) and (68) are real values. Thus, $\boldsymbol{\Psi}_u + \mathbf{j}\boldsymbol{\Psi}_v$ can be spectrally decomposed as

$$\boldsymbol{\Psi}_u + \mathbf{j}\boldsymbol{\Psi}_v = \mathbf{T}^{-1}(\boldsymbol{\Omega}_u + \mathbf{j}\boldsymbol{\Omega}_v)\mathbf{T}. \tag{69}$$

Accordingly, $\bar{u}_k$ and $\bar{v}_k$ for $1 \le k \le K$ can be estimated based on the eigenvalues of (69), denoted by ϖ_k for $1 \le k \le K$, as

$$\widehat{\bar{u}}_k = 2\tan^{-1}\left(\Re\{\varpi_k\}\right), \tag{70}$$

$$\widehat{\bar{v}}_k = 2\tan^{-1}\left(\Im\{\varpi_k\}\right). \tag{71}$$

From the definition of spatial frequency, we obtain the final estimates of the central DOAs as

$$\widehat{\bar{\phi}}_k = \tan^{-1}\left(\widehat{\bar{v}}_k / \widehat{\bar{u}}_k\right), \tag{72}$$

$$\widehat{\bar{\theta}}_k = \sin^{-1}\sqrt{\left(\frac{\widehat{\bar{u}}_k\lambda}{2\pi d}\right)^2 + \left(\frac{\widehat{\bar{v}}_k\lambda}{2\pi d}\right)^2}. \tag{73}$$

C. ESTIMATION OF ANGULAR SPREADS

After the DOA estimation, the search procedure is reduced to one that searches for the two angular spreads of each CD source, namely, the last two parameters in $\boldsymbol{\mu}_k = \left[\widehat{\bar{\phi}}_k\,\widehat{\bar{\theta}}_k\,\sigma_{\phi_k}\,\sigma_{\theta_k}\right]^T$. The correlation matrix of the array's signal vector $\mathbf{x}(t)$ of (10) is given by

$$\mathbf{R}_x = \mathbb{E}\{\mathbf{x}(t)\mathbf{x}^H(t)\} \approx \mathbf{E}_s\boldsymbol{\Sigma}_s\mathbf{E}_s^H + \sigma_n^2\mathbf{E}_n\mathbf{E}_n^H, \tag{74}$$

where $\boldsymbol{\Sigma}_s \in \mathbb{C}^{K \times K}$ is the diagonal matrix whose diagonal elements are the K largest eigenvalues of $\mathbf{R}_x$, and $\mathbf{E}_s \in \mathbb{C}^{MN \times K}$ whose columns are the eigenvectors associated with $\boldsymbol{\Sigma}_s$, i.e., $\mathbf{E}_s$ spans the signal subspace, while $\mathbf{E}_n \in \mathbb{C}^{MN \times (MN-K)}$ contains $(MN - K)$ eigenvectors associated with the noise subspace. Using the DSPE algorithm given in [22], the estimation of the angular spreads can be obtained as

$$\{\widehat{\sigma}_{\phi_k}, \widehat{\sigma}_{\theta_k}\} = \arg\max_{\sigma_{\phi_k},\sigma_{\theta_k}} \frac{1}{\|\mathbf{b}^H(\boldsymbol{\mu}_k)\mathbf{E}_n\|^2}. \tag{75}$$

But this process requires spectrum peak searching. To the best of our knowledge, almost all the research on the estimation of angular spreads involves spectrum peak searching [25], [26], which imposes excessive computational complexity.

We now discuss how to estimate angular spreads without high-complexity spectrum peak searching. As the transmitted signal and the noise are uncorrelated, the covariance matrix of $\mathbf{x}(t)$ can be expressed as

$$\mathbf{R}_x = \mathbb{E}\{\mathbf{x}(t)\mathbf{x}^H(t)\} = \sum_{k=1}^{K} P_k\mathbf{b}(\boldsymbol{\mu}_k)\mathbf{b}^H(\boldsymbol{\mu}_k) + \sigma_n^2\mathbf{I}_{MN}$$

$$= \sum_{k=1}^{K} P_k\Xi_k + \sigma_n^2\mathbf{I}_{MN}, \tag{76}$$

where

$$\Xi_k = \mathbf{b}(\boldsymbol{\mu}_k)\mathbf{b}^H(\boldsymbol{\mu}_k)$$
$$\approx \left(\mathbf{a}(\bar{\phi}_k, \bar{\theta}_k)\mathbf{a}^H(\bar{\phi}_k, \bar{\theta}_k)\right) \odot \mathbf{E}_k = \mathbf{D}_k\mathbf{E}_k\mathbf{D}_k^H, \tag{77}$$

with the diagonal matrix $\mathbf{D}_k \in \mathbb{C}^{MN \times MN}$ whose diagonal elements are the elements of $\mathbf{a}(\bar{\phi}_k, \bar{\theta}_k)$, and $\mathbf{E}_k \in \mathbb{R}^{MN \times MN}$ whose (p, q)th entry is given by $[\mathbf{E}_k]_{p,q} = [\mathbf{h}(\boldsymbol{\mu}_k)]_p[\mathbf{h}(\boldsymbol{\mu}_k)]_q$. From (11) to (14), we have $\underline{c}_k^p, l_k^p, g_k^p, o_k^p$, where $p = (m_p - 1)N + n_p$ with $m_p = 1, 2, \cdots, M$ and $n_p = 1, 2, \cdots, N$. Similarly, we have $\underline{c}_k^q, l_k^q, g_k^q$ and o_k^q, where $q = (m_q-1)N+n_q$ with $m_q = 1, 2, \cdots, M$ and $n_q = 1, 2, \cdots, N$. Noting the approximate relationship (19), we have

$$[\mathbf{E}_k]_{p,q} = e^{\gamma\sigma_{\phi_k}^2\left[(c_k^p)^2+(l_k^p)^2+(c_k^q)^2+(l_k^q)^2\right]}$$
$$\times e^{\gamma\sigma_{\theta_k}^2\left[(g_k^p)^2+(o_k^p)^2+(g_k^q)^2+(o_k^q)^2\right]}, \tag{78}$$

where $p, q = 1, 2, \cdots, MN$, and $\gamma = -2\pi^2\left(\frac{d}{\lambda}\right)^2$. By defining $\underline{\mathbf{P}} = [P_1\mathbf{I}_{MN}\,P_2\mathbf{I}_{MN}\cdots P_K\mathbf{I}_{MN}] \in \mathbb{R}^{MN \times KMN}$ and $\underline{\Xi} = [\Xi_1^T\,\Xi_2^T\cdots\Xi_K^T]^T \in \mathbb{C}^{KMN \times MN}$, we can rewrite (76) as

$$\mathbf{R}_x = \underline{\mathbf{P}}\,\underline{\Xi} + \sigma_n^2\mathbf{I}_{MN}. \tag{79}$$

Then, we can obtain

$$\widehat{\underline{\Xi}} = \underline{\mathbf{P}}^{\dagger}\left(\mathbf{R}_x - \widehat{\sigma}_n^2 \mathbf{I}_{MN}\right), \tag{80}$$

where $\widehat{\sigma}_n^2$ is the noise variance estimate, which is the average of the $MN - K$ smallest eigenvalues of $\mathbf{R}_x$. In practice, the covariance matrix $\mathbf{R}_x$ is estimated as

$$\widehat{\mathbf{R}}_x = \frac{1}{T}\sum_{t=1}^{T}\mathbf{x}(t)\mathbf{x}^H(t). \tag{81}$$

The extraction of the block $\widehat{\Xi}_k$ from $\widehat{\underline{\Xi}}$ is described by

$$\widehat{\Xi}_k^T = \widehat{\underline{\Xi}}^T\left(\boldsymbol{\epsilon}_k \otimes \mathbf{I}_{MN}\right), \tag{82}$$

where the $K \times 1$ column vector $\boldsymbol{\epsilon}_k$ is given by: for $1 \leq i \leq K$, $[\boldsymbol{\epsilon}_k]_i = 1$ if $i = k$; otherwise, $[\boldsymbol{\epsilon}_k]_i = 0$. Based on the estimated $\widehat{\phi}_k$ and $\widehat{\theta}_k$, we obtain $\widehat{\mathbf{D}}_k$ and then the estimate

$$\widehat{\mathbf{E}}_k = \left(\widehat{\mathbf{D}}_k\right)^{-1}\widehat{\Xi}_k\left(\widehat{\mathbf{D}}_k^H\right)^{-1}. \tag{83}$$

With $\widehat{\bar{\phi}}_k$ and $\widehat{\bar{\theta}}_k$, we also obtain the following coefficients

$$\left[\mathbf{r}_{\sigma_{\phi}}\left(\widehat{\bar{\phi}}_k, \widehat{\bar{\theta}}_k\right)\right]_{p,q} = \left(\underline{c}_k^p\right)^2 + \left(\underline{l}_k^p\right)^2 + \left(\underline{c}_k^q\right)^2 + \left(\underline{l}_k^q\right)^2, \tag{84}$$

$$\left[\mathbf{r}_{\sigma_{\theta}}\left(\widehat{\bar{\phi}}_k, \widehat{\bar{\theta}}_k\right)\right]_{p,q} = \left(\underline{g}_k^p\right)^2 + \left(\underline{o}_k^p\right)^2 + \left(\underline{g}_k^q\right)^2 + \left(\underline{o}_k^q\right)^2. \tag{85}$$

Then, we rearrange (78) as

$$\ln\left(\left[\widehat{\mathbf{E}}_k\right]_{p,q}\right)/\gamma = \sigma_{\phi_k}^2\left[\mathbf{r}_{\sigma_{\phi}}\left(\widehat{\bar{\phi}}_k, \widehat{\bar{\theta}}_k\right)\right]_{p,q} + \sigma_{\theta_k}^2\left[\mathbf{r}_{\sigma_{\theta}}\left(\widehat{\bar{\phi}}_k, \widehat{\bar{\theta}}_k\right)\right]_{p,q}, \tag{86}$$

and map the $MN \times MN$ matrix $\ln\left(\widehat{\mathbf{E}}_k\right)/\gamma$ onto an $(MN)^2 \times 1$ vector as

$$\begin{aligned}\widehat{\mathbf{g}}_k &= \mathbf{vec}\left\{\ln\left(\widehat{\mathbf{E}}_k\right)/\gamma\right\} \\ &= \sigma_{\phi_k}^2 \mathbf{vec}\left\{\mathbf{r}_{\sigma_{\phi}}\left(\widehat{\bar{\phi}}_k, \widehat{\bar{\theta}}_k\right)\right\} + \sigma_{\theta_k}^2 \mathbf{vec}\left\{\mathbf{r}_{\sigma_{\theta}}\left(\widehat{\bar{\phi}}_k, \widehat{\bar{\theta}}_k\right)\right\},\end{aligned} \tag{87}$$

where the function operator $\ln( )$ operates on $\widehat{\mathbf{E}}_k$ element-wise. By defining

$$\boldsymbol{\sigma}_k = \left[\sigma_{\phi_k}^2 \ \sigma_{\theta_k}^2\right]^T, \tag{88}$$

$$\widehat{\mathbf{W}}_k = \left[\mathbf{vec}\left\{\mathbf{r}_{\sigma_{\phi}}\left(\widehat{\bar{\phi}}_k, \widehat{\bar{\theta}}_k\right)\right\} \ \mathbf{vec}\left\{\mathbf{r}_{\sigma_{\theta}}\left(\widehat{\bar{\phi}}_k, \widehat{\bar{\theta}}_k\right)\right\}\right]. \tag{89}$$

we readily obtain the estimate of the two angular spreads as

$$\widehat{\boldsymbol{\sigma}}_k = \widehat{\mathbf{W}}_k^{\dagger}\widehat{\mathbf{g}}_k. \tag{90}$$

The complete proposed algorithm for estimating the central DOAs and angular spreads is summarized in Algorithm 1.

D. SIGNAL RECONSTRUCTION

Having obtained the estimates of the central DOAs and angular spreads, we can calculate the generalized steering matrix $\mathbf{B}$. Then, according to (10), we may obtain the signal reconstruction using, for example, the LS estimate of

$$\widehat{\mathbf{s}}(t) = \left(\mathbf{B}^H\mathbf{B}\right)^{-1}\mathbf{B}^H\mathbf{x}(t). \tag{91}$$

However, the inverse operation is challenging in the massive MIMO system since the complexity of computing $\left(\mathbf{B}^H\mathbf{B}\right)^{-1}$

Algorithm 1 Estimation of the Central DOAs and Angular Spreads

1: Calculate the received signal $\mathbf{Y} = \left(\mathbf{Q}_M^H \otimes \mathbf{Q}_N^H\right)\mathbf{X}$;
2: Compute $\mathbf{E}_{\Lambda}$ as the K largest left singular vectors of $[\Re\{\mathbf{Y}\} \ \Im\{\mathbf{Y}\}]$;
3: Compute $\boldsymbol{\Psi}_u$ and $\boldsymbol{\Psi}_v$ according to (67) and (68);
4: Compute the eigenvalues ϖ_k for $1 \leq k \leq K$ of $\boldsymbol{\Psi}_u + j\boldsymbol{\Psi}_v$;
5: Compute the spatial frequency estimates $\widehat{u}_k$ and $\widehat{v}_k$ for $1 \leq k \leq K$ according to (70) and (71);
6: Estimate the central DOAs $\widehat{\phi}_k$ and $\widehat{\theta}_k$ for $1 \leq k \leq K$ according to (72) and (73);
7: Compute the covariance matrix $\widehat{\mathbf{R}}_x$ of the received signal using (81);
8: Based on $\widehat{\bar{\phi}}_k$ and $\widehat{\bar{\theta}}_k$ for $1 \leq k \leq K$ obtained in step 6, estimate $\widehat{\mathbf{E}}_k$ according to (83), and calculate $\mathbf{r}_{\sigma_{\phi}}\left(\widehat{\bar{\phi}}_k, \widehat{\bar{\theta}}_k\right)$ and $\mathbf{r}_{\sigma_{\theta}}\left(\widehat{\bar{\phi}}_k, \widehat{\bar{\theta}}_k\right)$ using (84) and (85);
9: Estimate the angular spreads $\widehat{\sigma}_{\phi_k}^2$ and $\widehat{\sigma}_{\theta_k}^2$ for $1 \leq k \leq K$ according to (90).

---

is excessive. Hence, alternative low-complexity signal reconstruction techniques are desired. First, we give the following theorem.

Theorem 2: For a URA with azimuth and elevation DOAs drawn independently from a continuous distribution, the array response vectors are orthogonal when the number of antenna elements, MN, tends to infinity; that is,

$$\lim_{MN \to \infty}\frac{1}{MN}\mathbf{B}^H\mathbf{B} = \mathbf{I}_K. \tag{92}$$

Proof: See Appendix A. ∎

Since in a massive MIMO, MN is sufficiently large, we have $\frac{1}{MN}\mathbf{B}^H\mathbf{B} \approx \mathbf{I}_K$ according to Theorem 2. Therefore, we have the following low-complexity signal reconstruction

$$\widehat{\mathbf{s}}(t) \approx \frac{1}{MN}\mathbf{B}^H\mathbf{x}(t), \tag{93}$$

which does not involve matrix inversion.

IV. ANALYSIS OF THE PROPOSED ESTIMATOR
A. APPROXIMATE CRLB OF THE PROPOSED ESTIMATOR
First, we collect all the parameters to be estimated in the following parameter vector

$$\boldsymbol{\omega} = \left[\boldsymbol{\omega}_{\bar{\phi}}^T \ \boldsymbol{\omega}_{\bar{\theta}}^T \ \boldsymbol{\omega}_{\sigma_{\phi}}^T \ \boldsymbol{\omega}_{\sigma_{\theta}}^T\right]^T \in \mathbb{R}^{4K \times 1}, \tag{94}$$

where

$$\begin{cases}\boldsymbol{\omega}_{\bar{\phi}} = \left[\bar{\phi}_1 \ \bar{\phi}_2 \cdots \bar{\phi}_K\right]^T, \\ \boldsymbol{\omega}_{\bar{\theta}} = \left[\bar{\theta}_1 \ \bar{\theta}_2 \cdots \bar{\theta}_K\right]^T, \\ \boldsymbol{\omega}_{\sigma_{\phi}} = \left[\sigma_{\phi_1} \ \sigma_{\phi_2} \cdots \sigma_{\phi_K}\right]^T, \\ \boldsymbol{\omega}_{\sigma_{\theta}} = \left[\sigma_{\theta_1} \ \sigma_{\theta_2} \cdots \sigma_{\theta_K}\right]^T.\end{cases} \tag{95}$$

Further, define the expanded parameter vector

$$\bar{\boldsymbol{\omega}} = \left[\boldsymbol{\omega}^T \ \sigma_n^2\right]^T \in \mathbb{R}^{(4K+1) \times 1}. \tag{96}$$

TABLE 1. Complexity required in computing $\boldsymbol{\Psi}_u$ and $\boldsymbol{\Psi}_v$.

Operations	Real multiplications
$\mathbf{K}_1, \mathbf{K}_2$	$2\big((M-1)^2 M + M^2(M-1)\big)$
$\mathbf{K}_{u_1}, \mathbf{K}_{u_2}$	$2MN(M-1)$
$\mathbf{K}_{u_1}\mathbf{E}_\Lambda, \mathbf{K}_{u_2}\mathbf{E}_\Lambda$	$2MN^2(M-1)T$
$(\mathbf{K}_{u_1}\mathbf{E}_\Lambda)^\dagger$	$\frac{4}{3}K^3 + K^2(M-1)N$
$\boldsymbol{\Psi}_u$	$K^2(M-1)N$
$\mathbf{K}_3, \mathbf{K}_4$	$2\big((N-1)^2 N + N^2(N-1)\big)$
$\mathbf{K}_{v_1}, \mathbf{K}_{v_2}$	$2MN(N-1)$
$\mathbf{K}_{v_1}\mathbf{E}_\Lambda, \mathbf{K}_{v_2}\mathbf{E}_\Lambda$	$2M^2 N(N-1)T$
$(\mathbf{K}_{v_1}\mathbf{E}_\Lambda)^\dagger$	$\frac{4}{3}K^3 + K^2 M(N-1)$
$\boldsymbol{\Psi}_v$	$K^2 M(N-1)$

Given the Fisher information matrix

$$J_{\overline{\omega},\overline{\omega}} = \begin{bmatrix} J_{\omega,\omega} & J_{\omega,\sigma_n} \\ J_{\omega,\sigma_n}^T & J_{\sigma_n,\sigma_n} \end{bmatrix}, \quad (97)$$

where $J_{\omega,\omega} \in \mathbb{R}^{4K \times 4K}$, $J_{\omega,\sigma_n} \in \mathbb{R}^{4K \times 1}$ and $J_{\sigma_n,\sigma_n} \in \mathbb{R}$, the CRLB $C \in \mathbb{R}^{4K \times 4K}$ is expressed as [40]

$$C = \big(J_{\omega,\omega} - J_{\omega,\sigma_n} J_{\sigma_n,\sigma_n}^{-1} J_{\omega,\sigma_n}^T\big)^{-1}. \quad (98)$$

The derivation of the approximate FIM for (97) is presented in Appendix VI-B. Substituting this approximate FIM into (98) leads to the approximate CRLB for the estimator of $\boldsymbol{\omega}$.

B. COMPLEXITY ANALYSIS OF THE PROPOSED ESTIMATOR
1) COMPLEXITY OF ESTIMATING CENTRAL DOAs
Step 1 to Step 6 in Algorithm 1 estimate the central DOAs.

Since $\mathbf{Q}_M$ and $\mathbf{Q}_N$ are unitary matrices, computing $\mathbf{Q}_M^H \otimes \mathbf{Q}_N^H$ only requires $2N$ real multiplications. The number of real multiplications required to obtain $\mathbf{Y} = \mathbf{Q}_M^H \otimes \mathbf{Q}_N^H$ is given by $\frac{1}{2}T(MN)^2$. Therefore, the complexity of Step 1 is

$$C_1 \approx \frac{1}{2}T(MN)^2. \quad (99)$$

Step 2 involves the singular value decomposition of the real matrix $\boldsymbol{\Lambda}$, and the number of multiplications required is [41]

$$C_2 = \frac{17}{3}(MN)^3 + 2T(MN)^2. \quad (100)$$

The computational requirements of Step 3 are detailed in Table 1, where the complexity of the pseudo-inverse is from [42]. The number of real multiplications required in Step 3 C_3 is the sum of all the numbers in the righthand column of Table 1. As MN is very large, the complexity of Step 3 is approximately

$$C_3 \approx 4T(MN)^2. \quad (101)$$

Step 4 involves the EVD of the $K \times K$ matrix $\boldsymbol{\Psi}_u + j\boldsymbol{\Psi}_v$. With the QR algorithm, $20K^3$ real multiplications are required [41] and, therefore, the complexity of Step 4 is

$$C_4 = 20K^3. \quad (102)$$

The computational requirements of Step 5 and Step 6 are much smaller and can be ignored.

Thus, the complexity of our proposed estimator for the central DOAs, in terms of real multiplications, is $C_{Pro}^{DOA} = C_1 + C_2 + C_3 + C_4$. Since MN is very large, C_{Pro}^{DOA} is on the order of $\frac{17}{3}(MN)^3 + \frac{13T}{2}(MN)^2$, that is,

$$C_{Pro}^{DOA} = \mathsf{O}\left(\frac{17}{3}(MN)^3 + \frac{13T}{2}(MN)^2\right). \quad (103)$$

2) COMPLEXITY OF ESTIMATING ANGULAR SPREADS
Step 7 to Step 9 in Algorithm 1 estimate the angular spreads.

In Step 7, the covariance $\widehat{\mathbf{R}}_x$ is calculated, and the number of real multiplications required is given by

$$C_7 = 2T(MN)^2. \quad (104)$$

In Step 8, inverting the $MN \times MN$ real diagonal matrix $\widehat{\mathbf{D}}_k$ requires MN real multiplications. Since $\underline{\mathbf{P}}$ is a real sparse and row-full-rank matrix, $\underline{\mathbf{P}}^\dagger = \big((\underline{\mathbf{P}}\,\underline{\mathbf{P}}^H)^{-1}\underline{\mathbf{P}}\big)^H$, and the complexity of calculating $\underline{\mathbf{P}}^\dagger$ is $K(MN)^2 + (K+1)MN$. Calculating $\widehat{\mathbf{E}}_k$ via (83) requires $8(MN)^2$ real multiplications. Therefore, the complexity of Step 8 can be expressed as

$$C_8 \approx (K+8)(MN)^2. \quad (105)$$

The complexity of Step 9 is given by

$$C_9 \approx 6(MN)^2. \quad (106)$$

Consequently, after estimating the central DOAs, the complexity of our angular spreads estimator, expressed in terms of the number of real multiplications, is given by

$$C_{Pro}^{AS} = C_7 + C_8 + C_9 = \mathsf{O}\big((2T + K + 14)(MN)^2\big), \quad (107)$$

which is much smaller than C_{Pro}^{DOA}.

3) TOTAL COMPLEXITY OF THE PROPOSED ESTIMATOR
It is then obvious that in terms of the number of real multiplications required, the total computational complexity of the proposed estimator is given by

$$\begin{aligned} C_{Pro} &= C_{Pro}^{DOA} + C_{Pro}^{AS} \\ &= \mathsf{O}\left(\frac{17}{3}(MN)^3 + \left(\frac{17T}{2} + K + 14\right)(MN)^2\right). \end{aligned} \quad (108)$$

It can readily be seen that the computational complexity of the proposed estimator is dominated by the requirements of estimating the central DOAs.

C. COMPUTATIONAL COMPLEXITY OF OTHER ESTIMATORS
1) LS-ESPRIT
The classic LS-ESPRIT algorithm [10], [43] can only estimate the central DOAs, and the complexity of LS-ESPRIT quantified in terms of the number of real-valued multiplications, can be expressed as

$$C_{LS-EPSIRT}^{DOA} = \mathsf{O}\big(20(MN)^3 + 10T(MN)^2\big), \quad (109)$$

which is considerably higher than C_{Pro}^{DOA}.

2) DSPE

The DSPE algorithm [22] estimates both the central DOAs and the angular spreads. In terms of real multiplications, the total computational complexity required by the DSPE algorithm to estimate the central DOAs and angular spreads can be expressed by

$$C_{DSPE} = \mathrm{O}\big(20(MN)^3 + (D_1 + 2T)(MN)^2\big), \quad (110)$$

where $D_1 = D_{\bar{\phi}} D_{\bar{\theta}} D_{\sigma_\phi} D_{\sigma_\theta}$, and $D_{\bar{\phi}}$, $D_{\bar{\theta}}$, D_{σ_ϕ} and D_{σ_θ} denote the search times required to estimate the central azimuth and elevation DOAs and the azimuth and elevation angular spreads, respectively. The search dimension D_1 is usually very large. For example, the DSPE-like algorithm of [19] has $D_1 = \mathrm{O}(10^4)$, while the DSPE-like algorithm of [44] has $D_1 = \mathrm{O}(10^6)$. It can be seen that C_{DSPE} is significantly higher than C_{Pro}.

V. SIMULATION RESULTS

The performance of our proposed estimator for central DOAs estimation is compared to those of the LS-ESPRIT method [10], [43] and the DSPE method [19], [22], [44], while the performance of our proposed estimator for angular spreads estimation is compared to that of the DSPE approach.

A. SIMULATION SETUP

Simulations are conducted with a URA having $M = N$ and $d = \lambda/2$. Two equi-powered, uncorrelated CD sources are located at the central angles $(\bar{\phi}_1 = 30°, \bar{\theta}_1 = 15°)$ and $(\bar{\phi}_2 = 75°, \bar{\theta}_2 = 60°)$, and thus $K = 2$. The azimuth and the elevation angular spreads of the two sources are $\sigma_{\phi_k} = \sigma_{\theta_k} = \sigma = 1°$, $k = 1, 2$, and the noise variance is $\sigma_n^2 = 1$. The transmitted signals $s_k(t)$, $k = 1, 2$, are quadrature phase-shift keying modulated. The number of snapshots is $T = 500$. All the results are averaged over 1000 Monte-Carlo simulation experiments. We define the root mean square error (RMSE) of the estimator for $\boldsymbol{\varpi} \in \mathbb{C}^{K \times 1}$, where $\boldsymbol{\varpi}$ represents $\boldsymbol{\omega}_{\bar{\phi}}$, $\boldsymbol{\omega}_{\bar{\theta}}$, $\boldsymbol{\omega}_{\sigma_\phi}$ or $\boldsymbol{\omega}_{\sigma_\theta}$, by the following sample average

$$RMSE_{\boldsymbol{\varpi}} = \sqrt{\frac{1}{1000} \sum_{c=1}^{1000} \big\| \widehat{\boldsymbol{\varpi}}^{(c)} - \boldsymbol{\varpi} \big\|^2}, \quad (111)$$

where $\widehat{\boldsymbol{\varpi}}^{(c)}$ denotes the estimate of $\boldsymbol{\varpi}$ obtained in the cth Monte-Carlo trial.

For the DSPE approach, the search range of the central azimuth DOAs is set to $[\bar{\phi}_k - 2°, \bar{\phi}_k + 2°]$, $k = 1, 2$, and the search range of the central elevation DOAs is set to $[\bar{\theta}_k - 1°, \bar{\theta}_k + 1°]$, $k = 1, 2$, while the search range of the angular spreads is set to $[\sigma - 0.2°, \sigma + 0.2°]$. Moreover, the search step sizes of the DSPE used for the central DOAs and the angular spreads are $0.1°$ and $0.05°$, respectively.

B. COMPLEXITY COMPARISON

Given the simulation parameters of Section V-A, the search dimension of the DSPE is $D_1 = (41 \times 9)^2$, with $D_{\bar{\phi}} = D_{\bar{\theta}} = (2° - (-2°))/0.1° + 1 = 41$ and $D_{\sigma_\phi} = D_{\sigma_\theta} = (1.2° - 0.8°)/0.05° + 1 = 9$. Fig. 3 (a) depicts the computational
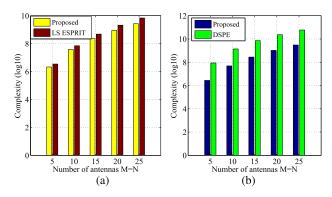

FIGURE 3. Comparison of complexity: (a) for estimating the central DOAs by the LS-ESPRIT and the proposed estimator, and (b) for estimating the central DOAs and angular spreads by the DSPE and the proposed estimator.
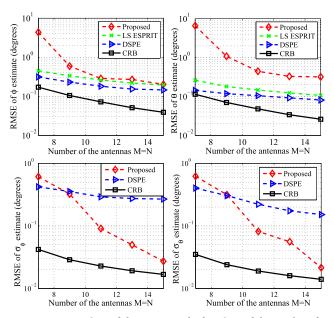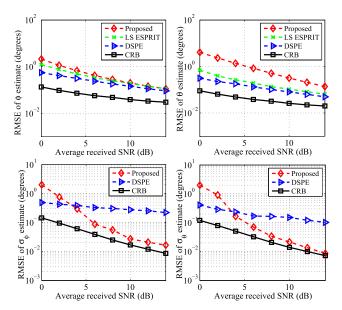

FIGURE 4. Comparison of the RMSEs as the functions of the number of BS antennas, given the SNR of 10 dB. The top two plots are the RMSEs of the three estimators for the central azimuth and elevation DOAs, and the bottom two plots are the RMSEs of the two estimators for the azimuth and elevation angular spreads.

complexities as the functions of the number of BS antennas required to estimate the central DOAs by the LS-ESPRIT and the proposed estimator, where the complexity is plotted in the base-10 logarithm. It can be seen that the LS-ESPRIT requires substantially higher complexity to estimate the central DOAs than the proposed estimator. Similarly, Fig. 3 (b) compares the computational complexities required by the DSPE and the proposed estimator for estimating the central DOAs and angular spreads. Clearly, our proposed estimator imposes dramatically lower complexity than the DSPE.

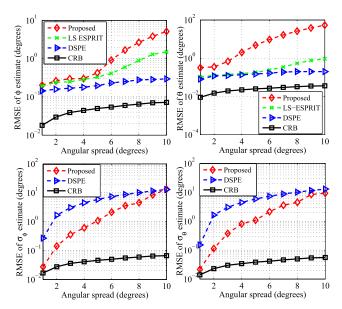### C. ESTIMATION ACCURACY COMPARISON

With the received signal-to-noise ratio (SNR) of each source set to 10 dB, Fig. 4 plots the four RMSEs, $RMSE_{\boldsymbol{\omega}_{\bar{\phi}}}$ and $RMSE_{\boldsymbol{\omega}_{\bar{\theta}}}$ as well as $RMSE_{\boldsymbol{\omega}_{\sigma_\phi}}$ and $RMSE_{\boldsymbol{\omega}_{\sigma_\theta}}$, as the functions of the number of BS antennas, obtained by different

FIGURE 5. Comparison of the RMSEs as the functions of the SNR, given the number of BS antennas $M \times N = 15 \times 15$. The top two plots are the RMSEs of the three estimators for the central azimuth and elevation DOAs, while the bottom two plots are the RMSEs of the two estimators for the azimuth and elevation angular spreads.

FIGURE 6. Comparison of the RMSEs as the functions of the angular spread σ, given a number of BS antennas $M \times N = 15 \times 15$ and SNR = 10 dB. The top two plots are the RMSEs of the three estimators for the central azimuth and elevation DOAs, while the bottom two plots are the RMSEs of the two estimators for the azimuth and elevation angular spreads.

estimators, where the CRLBs are also provided as benchmarks. In terms of the central azimuth and elevation angles, the LS-ESPRIT estimator has better estimation accuracy than our estimator, but the former imposes considerably higher complexity in estimating the central DOAs, while the DSPE estimator achieves the best estimation accuracy. For the azimuth and elevation angular spreads, our proposed estimator achieves better estimation accuracy than the DSPE estimator, except when the number of BS antennas is smaller than $M \times N = 9 \times 9 = 81$. This is remarkable, considering that our estimator imposes significantly lower complexity than the DSPE. The estimation accuracy of our proposed estimator improves significantly as the number of BS antennas increases. Therefore, our 2D unitary ESPRIT-based algorithm can better exploit the benefits of massive MIMO.

The reason why our proposed estimator outperforms the DSPE in estimating angular spread can be explained as follows. The high-complexity DSPE involves a discretized search, and the accuracy of its solution is fundamentally limited by the search step size in quantization. Furthermore, the search step size cannot be set to be too small, as this will lead to an unaffordable computational complexity. By contrast, our proposed estimator provides a closed-form solution to the angular spread estimation, which does not impose any quantization error. This closed-form angular spread estimate is calculated given the central DOA estimate. Observe from the top two plots of Fig. 4, the accuracy of the central DOA estimate by our estimator improves significantly as the number of BS antennas increases to over $M \times N = 81$. This also explains why the accuracy of our angular spread estimate is significantly better than that of the DSPE when the number

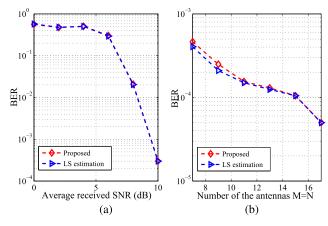of BS antennas is sufficiently large, as shown in the bottom two plots of Fig. 4.

In the second experiment, we set the number of BS antennas to $M \times N = 15 \times 15$ and vary the SNR. Fig. 5 depicts the corresponding four RMSEs obtained by different estimators. For the central elevation angle estimation, the accuracy of our proposed estimator is worse than those of the LS-ESPRIT and DSPE. However, for the azimuth and elevation angular spreads, our proposed estimator achieves significantly better estimation accuracy than the DSPE estimator when the received SNR is not less than 4 dB.

In the third experiment, we set the number of BS antennas to $M \times N = 15 \times 15$ and the SNR to 10 dB while varying the angular spread $\sigma_{\phi_k} = \sigma_{\theta_k} = \sigma$ from 1° to 10°. As shown in Fig. 6, in terms of the central azimuth and elevation angles, the estimation accuracy of our low-complexity estimator is worse than those of the LS-ESPRIT and DSPE estimators, but in terms of the estimation accuracy for the azimuth and elevation angular spreads, our proposed estimator outperforms the high-complexity DSPE estimator.

D. DATA RECONSTRUCTION COMPARISON
After estimating the central DOAs and angular spreads using our proposed estimator, the generalized steering matrix **B** can be calculated for signal reconstruction. We set the angular spread $\sigma_{\phi_k} = \sigma_{\theta_k} = \sigma$ to 1°. In Fig. 7 (a), we compare the bit error rate (BER) performance achieved by the high-complexity LS estimation (91) with the BER performance attained by our proposed low-complexity estimation (93), for various SNR values, where the number of BS antennas is

FIGURE 7. Comparison of the data detection performance of the two estimation methods: (a) varying the received SNR with the number of BS antennas fixed to $M \times N = 15 \times 15$, and (b) varying the number of BS antennas with the received SNR fixed to 10 dB.

fixed to $M \times N = 15 \times 15$. It can be observed that the BER of our low-complexity signal reconstruction method (93) is indistinguishable from the BER of the LS signal reconstruction method (91), which imposes much higher computational complexity than our proposed estimation method. By fixing the SNR to 10 dB and varying the number of BS antennas, Fig. 7 (b) depicts the BERs attained by the two signal reconstruction methods. It can be seen that when the number of BS antennas is greater than $M \times N = 10 \times 10$, the BERs of the two algorithms are indistinguishable. The results of Fig. 7 therefore also confirm Theorem 2, namely, given a sufficiently large number of BS antennas, MN, $\frac{1}{MN}\mathbf{B}^H\mathbf{B} = \mathbf{I}_K$ holds.

VI. CONCLUSIONS

A novel 2D unitary ESPRIT-based approach has been proposed for estimating the central DOAs and angular spreads of coherently distributed sources in massive MIMO systems, where the BS employs a large-scale URA. In contrast to the estimators available in the existing literature, such as the DSPE, our proposed estimator does not require complex search and matching processes and, consequently, it imposes dramatically lower computational complexity than the DSPE. Our simulation results have demonstrated that when estimating the central DOAs, the accuracy of our low-complexity estimator is worse than that of the high-complexity DSPE, but when estimating the angular spreads, our low-complexity estimator outperforms the high-complexity DSPE. We have also proposed a low-complexity signal reconstruction method, which has the same level of BER performance as the high-complexity LS estimation method for massive MIMO systems associated with a sufficiently large number of BS antennas.

APPENDIX
A. PROOF OF THEOREM 2

Proof: Consider the kth and k'th column vectors of $\mathbf{B}$, $\mathbf{b}(\boldsymbol{\mu}_k)$ and $\mathbf{b}(\boldsymbol{\mu}_{k'})$, where $k \neq k'$. Noting the approximate Kronecker product decomposition of the URA array response given in (28), we can express $\left|\mathbf{b}^H(\boldsymbol{\mu}_k)\mathbf{b}(\boldsymbol{\mu}_{k'})\right|$ approximately as given in (112), as shown at the bottom of this page, where the second approximate equality is the result of applying (23)

$$
\begin{aligned}
\left|\mathbf{b}^H(\boldsymbol{\mu}_k)\mathbf{b}(\boldsymbol{\mu}_{k'})\right| &\approx \left|\left(\mathbf{b}_x(\boldsymbol{\mu}_k)_{\frac{N+1}{2}} \otimes \mathbf{b}_y(\boldsymbol{\mu}_k)_{\frac{M+1}{2}}\right)^H \left(\mathbf{b}_x(\boldsymbol{\mu}_{k'})_{\frac{N+1}{2}} \otimes \mathbf{b}_y(\boldsymbol{\mu}_{k'})_{\frac{M+1}{2}}\right)\right| \\
&= \left|\left(\mathbf{b}_x^H(\boldsymbol{\mu}_k)_{\frac{N+1}{2}}\mathbf{b}_x(\boldsymbol{\mu}_{k'})_{\frac{N+1}{2}}\right) \otimes \left(\mathbf{b}_y^H(\boldsymbol{\mu}_k)_{\frac{M+1}{2}}\mathbf{b}_y(\boldsymbol{\mu}_{k'})_{\frac{M+1}{2}}\right)\right| \\
&\approx \left|\left(\sum_{m=1}^{M} e^{j\left(m-\frac{M+1}{2}\right)(\bar{u}_{k'}-\bar{u}_k)} e^{-\frac{2\pi^2 d^2}{\lambda^2}\left(\sigma_{\phi_k}^2 c_k^2 + \sigma_{\phi_{k'}}^2 c_{k'}^2\right)} e^{-\frac{2\pi^2 d^2}{\lambda^2}\left(\sigma_{\theta_k}^2 g_k^2 + \sigma_{\theta_{k'}}^2 g_{k'}^2\right)}\right)\right. \\
&\quad \left. \times \left(\sum_{n=1}^{N} e^{j\left(n-\frac{N+1}{2}\right)(\bar{v}_{k'}-\bar{v}_k)} e^{-\frac{2\pi^2 d^2}{\lambda^2}\left(\sigma_{\phi_k}^2 l_k^2 + \sigma_{\phi_{k'}}^2 l_{k'}^2\right)} e^{-\frac{2\pi^2 d^2}{\lambda^2}\left(\sigma_{\theta_k}^2 o_k^2 + \sigma_{\theta_{k'}}^2 o_{k'}^2\right)}\right)\right|. \quad (112)
\end{aligned}
$$

$$
\begin{aligned}
\left|\mathbf{b}^H(\boldsymbol{\mu}_k)\mathbf{b}(\boldsymbol{\mu}_{k'})\right| &\approx \left|\left(\sum_{m=1}^{M} x_1 x_2\, e^{j\left(m-\frac{M+1}{2}\right)(\bar{u}_{k'}-\bar{u}_k)}\right)\left(\sum_{n=1}^{N} y_1 y_2\, e^{j\left(n-\frac{N+1}{2}\right)(\bar{v}_{k'}-\bar{v}_k)}\right)\right| \\
&\leq \left|\left(\sum_{m=1}^{M} e^{j\left(m-\frac{M+1}{2}\right)(\bar{u}_{k'}-\bar{u}_k)}\right)\left(\sum_{n=1}^{N} e^{j\left(n-\frac{N+1}{2}\right)(\bar{v}_{k'}-\bar{v}_k)}\right)\right| \\
&= \frac{\left|e^{j\left(-\frac{M+1}{2}\right)(\bar{u}_{k'}-\bar{u}_k)}\left(1-e^{j(\bar{u}_{k'}-\bar{u}_k)M}\right)\right|}{\left|1-e^{j(\bar{u}_{k'}-\bar{u}_k)}\right|} \frac{\left|e^{j\left(-\frac{N+1}{2}\right)(\bar{v}_{k'}-\bar{v}_k)}\left(1-e^{j(\bar{v}_{k'}-\bar{v}_k)N}\right)\right|}{\left|1-e^{j(\bar{v}_{k'}-\bar{v}_k)}\right|} \\
&\leq \frac{4}{\left|1-e^{j(\bar{u}_{k'}-\bar{u}_k)}\right|\left|1-e^{j(\bar{v}_{k'}-\bar{v}_k)}\right|}. \quad (113)
\end{aligned}
$$

to (26) as well as (20). By denoting

$$x_1 = e^{-\frac{2\pi^2 d^2}{\lambda^2}\left(\sigma_{\phi_k}^2 c_k^2 + \sigma_{\phi_{k'}}^2 c_{k'}^2\right)},$$

$$x_2 = e^{-\frac{2\pi^2 d^2}{\lambda^2}\left(\sigma_{\theta_k}^2 g_k^2 + \sigma_{\phi_{k'}}^2 g_{k'}^2\right)},$$

$$y_1 = e^{-\frac{2\pi^2 d^2}{\lambda^2}\left(\sigma_{\phi_k}^2 l_k^2 + \sigma_{\phi_{k'}}^2 l_{k'}^2\right)},$$

$$y_2 = e^{-\frac{2\pi^2 d^2}{\lambda^2}\left(\sigma_{\theta_k}^2 o_k^2 + \sigma_{\theta_{k'}}^2 o_{k'}^2\right)},$$

we can rewrite (112) as (113), as shown at the bottom of the previous page. The third equality holds in (113) because $\bar{\phi}_{k'}$ and $\bar{\phi}_k$ as well as $\bar{\theta}_{k'}$ and $\bar{\theta}_k$ are chosen independently from a continuous distribution. Consequently, $\bar{u}_{k'} - \bar{u}_k \neq 0$ as well as $\bar{v}_{k'} - \bar{v}_k \neq 0$ with probability equal to one. Therefore, the two geometric series in (113) have ratios $e^{j(\bar{u}_{k'} - \bar{u}_k)} \neq 1$ and $e^{j(\bar{v}_{k'} - \bar{v}_k)} \neq 1$. From (113), we have

$$\lim_{MN \to \infty} \frac{1}{MN}\left|\mathbf{b}^H(\boldsymbol{\mu}_k)\mathbf{b}(\boldsymbol{\mu}_{k'})\right| = 0. \qquad (114)$$

On the other hand, it is straightforward to see that

$$\frac{1}{MN}\left|\mathbf{b}^H(\boldsymbol{\mu}_k)\mathbf{b}(\boldsymbol{\mu}_k)\right| = 1. \qquad (115)$$

This proves (92). ■

B. DERIVATION OF APPROXIMATE FIM
Recalling the correction matrix $\mathbf{R}_x$ of the array signal vector $\mathbf{x}(t)$, the (i, i')th element of the FIM $\boldsymbol{J}_{\bar{\omega},\bar{\omega}}$ is defined as [40]

$$\left[\boldsymbol{J}_{\bar{\omega},\bar{\omega}}\right]_{i,i'} = T\, tr\left(\mathbf{R}_x^{-1}\frac{\partial \mathbf{R}_x}{\partial[\bar{\omega}]_i}\mathbf{R}_x^{-1}\frac{\partial \mathbf{R}_x}{\partial[\bar{\omega}]_{i'}}\right), \qquad (116)$$

where $i, i' = 1, 2, \cdots, 4K + 1$. To explicitly calculate $\partial \mathbf{R}_x/\partial[\bar{\omega}]_i$ for $1 \leq i \leq 4K$, we define the transformation

$k = 1 + \lfloor (i-1)/4 \rfloor$. Based on (76) and (77), we obtain all the partial derivatives, which are

$$\frac{\partial \mathbf{R}_x}{\partial \bar{\phi}_k} \approx P_k\left(\mathbf{D}_{\bar{\phi}_k}\mathbf{D}_k\mathbf{E}_k\mathbf{D}_k^H - \mathbf{D}_k\mathbf{E}_k\mathbf{D}_k^H\mathbf{D}_{\bar{\phi}_k}, \right.$$
$$\left. + \mathbf{D}_k(\mathbf{E}_k \odot \mathbf{E}_{\bar{\phi}_k})\mathbf{D}_k^H\right), \qquad (117)$$

$$\frac{\partial \mathbf{R}_x}{\partial \bar{\theta}_k} \approx P_k\left(\mathbf{D}_{\bar{\theta}_k}\mathbf{D}_k\mathbf{E}_k\mathbf{D}_k^H - \mathbf{D}_k\mathbf{E}_k\mathbf{D}_k^H\mathbf{D}_{\bar{\theta}_k} \right.$$
$$\left. + \mathbf{D}_k(\mathbf{E}_k \odot \mathbf{E}_{\bar{\theta}_k})\mathbf{D}_k^H\right), \qquad (118)$$

$$\frac{\partial \mathbf{R}_x}{\partial \sigma_{\phi_k}} \approx P_k\left(\mathbf{D}_k(\mathbf{E}_k \odot \mathbf{E}_{\sigma_{\phi_k}})\mathbf{D}_k^H\right), \qquad (119)$$

$$\frac{\partial \mathbf{R}_x}{\partial \sigma_{\theta_k}} \approx P_k\left(\mathbf{D}_k(\mathbf{E}_k \odot \mathbf{E}_{\sigma_{\theta_k}})\mathbf{D}_k^H\right), \qquad (120)$$

for $1 \leq k \leq K$, and for $i = 4K + 1$

$$\frac{\partial \mathbf{R}_x}{\partial \sigma_n^2} \approx \mathbf{I}_{MN}, \qquad (121)$$

where the diagonal matrices $\mathbf{D}_{\bar{\phi}_k}$ and $\mathbf{D}_{\bar{\theta}_k}$ are specified by

$$\left[\mathbf{D}_{\bar{\phi}_k}\right]_{p,p} = j2\pi\frac{d}{\lambda}\sin\bar{\theta}_k\left(-\left(m_p - \frac{M+1}{2}\right)\sin\bar{\phi}_k \right.$$
$$\left. + \left(n_p - \frac{N+1}{2}\right)\cos\bar{\phi}_k\right), \qquad (122)$$

$$\left[\mathbf{D}_{\bar{\theta}_k}\right]_{p,p} = j2\pi\frac{d}{\lambda}\cos\bar{\theta}_k\left(\left(m_p - \frac{M+1}{2}\right)\cos\bar{\phi}_k \right.$$
$$\left. + \left(n_p - \frac{N+1}{2}\right)\sin\bar{\phi}_k\right), \qquad (123)$$

while the matrices $\mathbf{E}_{\bar{\phi}_k}$, $\mathbf{E}_{\bar{\theta}_k}$, $\mathbf{E}_{\sigma_{\phi_k}}$ and $\mathbf{E}_{\sigma_{\theta_k}}$ are specified in (124) to (127), as shown at the bottom of this page, respectively. In (122) to (127), we have $p, q = 1, 2, \cdots, MN$, while m_p and n_p denote the numbers of azimuth antenna

$$\left[\mathbf{E}_{\bar{\phi}_k}\right]_{p,q} = 2\gamma\sigma_{\theta_k}^2\sin\bar{\phi}_k\cos\bar{\phi}_k\cos^2\bar{\theta}_k\left(-\left(m_p - \frac{M+1}{2}\right)^2 - \left(m_q - \frac{M+1}{2}\right)^2 + \left(n_p - \frac{N+1}{2}\right)^2 + \left(n_q - \frac{N+1}{2}\right)^2\right)$$
$$+ 2\gamma\sigma_{\phi_k}^2\sin\bar{\phi}_k\cos\bar{\phi}_k\sin^2\bar{\theta}_k\left(\left(m_p - \frac{M+1}{2}\right)^2 + \left(m_q - \frac{M+1}{2}\right)^2 - \left(n_p - \frac{N+1}{2}\right)^2 - \left(n_q - \frac{N+1}{2}\right)^2\right), \qquad (124)$$

$$\left[\mathbf{E}_{\bar{\theta}_k}\right]_{p,q} = -2\gamma\sigma_{\theta_k}^2\sin\bar{\theta}_k\cos\bar{\theta}_k\left(\left(\left(m_p - \frac{M+1}{2}\right)^2 + \left(m_q - \frac{M+1}{2}\right)^2\right)\cos^2\bar{\phi}_k + \left(\left(n_p - \frac{N+1}{2}\right)^2 + \left(n_q - \frac{N+1}{2}\right)^2\right)\sin^2\bar{\phi}_k\right)$$
$$+ 2\gamma\sigma_{\phi_k}^2\sin\bar{\theta}_k\cos\bar{\theta}_k\left(\left(\left(m_p - \frac{M+1}{2}\right)^2 + \left(m_q - \frac{M+1}{2}\right)^2\right)\sin^2\bar{\phi}_k + \left(\left(n_p - \frac{N+1}{2}\right)^2 + \left(n_q - \frac{N+1}{2}\right)^2\right)\cos^2\bar{\phi}_k\right), \qquad (125)$$

$$\left[\mathbf{E}_{\sigma_{\phi_k}}\right]_{p,q} = 2\gamma\sigma_{\phi_k}\left(\left(m_p - \frac{M+1}{2}\right)^2\sin^2\bar{\phi}_k\sin^2\bar{\theta}_k + \left(n_p - \frac{N+1}{2}\right)^2\cos^2\bar{\phi}_k\sin^2\bar{\theta}_k\right.$$
$$\left. + \left(m_q - \frac{M+1}{2}\right)^2\sin^2\bar{\phi}_k\sin^2\bar{\theta}_k + \left(n_q - \frac{N+1}{2}\right)^2\cos^2\bar{\phi}_k\sin^2\bar{\theta}_k\right), \qquad (126)$$

$$\left[\mathbf{E}_{\sigma_{\theta_k}}\right]_{p,q} = 2\gamma\sigma_{\theta_k}\left(\left(m_p - \frac{M+1}{2}\right)^2\cos^2\bar{\phi}_k\cos^2\bar{\theta}_k + \left(n_p - \frac{N+1}{2}\right)^2\sin^2\bar{\phi}_k\cos^2\bar{\theta}_k\right.$$
$$\left. + \left(m_q - \frac{M+1}{2}\right)^2\cos^2\bar{\phi}_k\cos^2\bar{\theta}_k + \left(n_q - \frac{N+1}{2}\right)^2\sin^2\bar{\phi}_k\cos^2\bar{\theta}_k\right). \qquad (127)$$

elements and elevation antenna elements, respectively, when the total number of antenna elements is p. The symbols n_p and n_q have the similar definitions.

REFERENCES

[1] E. Hossain and M. Hasan, "5G cellular: Key enabling technologies and research challenges," *IEEE Instrum. Meas. Mag.*, vol. 18, no. 3, pp. 11–21, Jun. 2015.

[2] S. Yang and L. Hanzo, "Fifty years of MIMO detection: The road to large-scale MIMOs," *IEEE Commun. Surveys Tuts.*, vol. 17, no. 4, pp. 1941–1988, 4th Quart., 2015.

[3] S. Yang, C. Zhou, T. Lv, and L. Hanzo, "Large-scale MIMO is capable of eliminating power-thirsty channel coding for wireless transmission of HEVC/H.265 video," *IEEE Wireless Commun.*, vol. 23, no. 3, pp. 57–63, Jun. 2016.

[4] T. L. Marzetta, "Noncooperative cellular wireless with unlimited numbers of base station antennas," *IEEE Trans. Wireless Commun.*, vol. 9, no. 11, pp. 3590–3600, Nov. 2010.

[5] F. Rusek *et al.*, "Scaling up MIMO: Opportunities and challenges with very large arrays," *IEEE Signal Process. Mag.*, vol. 30, no. 1, pp. 40–60, Jan. 2013.

[6] H. Krim and M. Viberg, "Two decades of array signal processing research: The parametric approach," *IEEE Signal Process. Mag.*, vol. 13, no. 4, pp. 67–94, Jul. 1996.

[7] J. Capon, "Maximum-likelihood spectral estimation," in *Nonlinear Methods of Spectral Analysis*, S. Haykin Ed. Berlin, Germany: Springer-Verlag, 1983, pp. 155–179.

[8] R. O. Schmidt, "Multiple emitter location and signal parameter estimation," *IEEE Trans. Antennas Propag.*, vol. 34, no. 3, pp. 276–280, Mar. 1986.

[9] A. Barabell, "Improving the resolution performance of eigenstructure-based direction-finding algorithms," in *Proc. ICASSP*, vol. 8. Boston, MA, USA, Apr. 1983, pp. 336–339.

[10] R. Roy and T. Kailath, "ESPRIT-estimation of signal parameters via rotational invariance techniques," *IEEE Trans. Acoust., Speech, Signal Process.*, vol. 37, no. 7, pp. 984–995, Jul. 1989.

[11] M. Haardt and J. A. Nossek, "Unitary ESPRIT: How to obtain increased estimation accuracy with a reduced computational burden," *IEEE Trans. Signal Process.*, vol. 43, no. 5, pp. 1232–1242, May 1995.

[12] A. Wang, L. Liu, and J. Zhang, "Low complexity direction of arrival (DoA) estimation for 2D massive MIMO systems," in *Proc. Globecom Workshops*, Anaheim, CA, USA, Dec. 2012, pp. 703–707.

[13] Y. Zhu, L. Liu, A. Wang, K. Sayana, and J. C. Zhang, "DoA estimation and capacity analysis for 2D active massive MIMO systems," in *Proc. ICC*, Budapest, Hungary, Jun. 2013, pp. 4630–4634.

[14] K.-Y. Yang, J.-Y. Wu, and W.-H. Li, "A low-complexity direction-of-arrival estimation algorithm for full-dimension massive MIMO systems," in *Proc. ICCS*, Macau, China, Nov. 2014, pp. 472–476.

[15] L. Liu, Y. Li, and J. Zhang, "DoA estimation and achievable rate analysis for 3D millimeter wave massive MIMO systems," in *Proc. SPAWC*, Toronto, ON, Canada, Jun. 2014, pp. 6–10.

[16] F. Wen and C. Liang, "Improved tensor-MODE based direction-of-arrival estimation for massive MIMO systems," *IEEE Commun. Lett.*, vol. 19, no. 12, pp. 2182–2185, Dec. 2015.

[17] L. Cheng, Y.-C. Wu, J. Zhang, and L. Liu, "Subspace identification for DOA estimation in massive/full-dimension MIMO systems: Bad data mitigation and automatic source enumeration," *IEEE Trans. Signal Process.*, vol. 63, no. 22, pp. 5897–5909, Nov. 2015.

[18] T. Wang, B. Ai, R. He, and Z. Zhong, "Two-dimension direction-of-arrival estimation for massive MIMO systems," *IEEE Access*, vol. 3, pp. 2122–2129, 2015.

[19] A. Hu, T. Lv, H. Gao, Z. Zhang, and S. Yang, "An ESPRIT-based approach for 2-D localization of incoherently distributed sources in massive MIMO systems," *IEEE J. Sel. Topics Signal Process.*, vol. 8, no. 5, pp. 996–1011, Oct. 2014.

[20] T. Lv, F. Tan, H. Gao, and S. Yang, "A beamspace approach for 2-D localization of incoherently distributed sources in massive MIMO systems," *Signal Process.*, vol. 121, pp. 30–45, Apr. 2016.

[21] L. Wan, G. Han, J. Jiang, J. J. P. C. Rodrigues, N. Feng, and T. Zhu, "DOA estimation for coherently distributed sources considering circular and noncircular signals in massive MIMO systems," *IEEE Syst. J.*, vol. 11, no. 1, pp. 41–49, Mar. 2017.

[22] S. Valaee, B. Champagne, and P. Kabal, "Parametric localization of distributed sources," *IEEE Trans. Signal Process.*, vol. 43, no. 9, pp. 2144–2153, Sep. 1995.

[23] S. Shahbazpanahi, S. Valaee, and M. H. Bastani, "Distributed source localization using ESPRIT algorithm," *IEEE Trans. Signal Process.*, vol. 49, no. 10, pp. 2169–2178, Oct. 2001.

[24] Y. Han and J. Wang, "The central DOA estimation algorithm based on support vector regression for coherently distributed source," *J. Softw.*, vol. 7, no. 12, pp. 2710–2716, Dec. 2012.

[25] T. Trump and B. Ottersten, "Estimation of nominal direction of arrival and angular spread using an array of sensors," *Signal Process.*, vol. 50, nos. 1–2, pp. 57–69, Apr. 1996.

[26] B. T. Sieskul, "An asymptotic maximum likelihood for joint estimation of nominal angles and angular spreads of multiple spatially distributed sources," *IEEE Trans. Veh. Technol.*, vol. 59, no. 3, pp. 1534–1538, Mar. 2010.

[27] B. Ottersten, P. Stoica, and R. Roy, "Covariance matching estimation techniques for array signal processing applications," *Digit. Signal Process.*, vol. 8, no. 3, pp. 185–210, Jul. 1998.

[28] O. Besson and P. Stoica, "Decoupled estimation of DOA and angular spread for a spatially distributed source," *IEEE Trans. Signal Process.*, vol. 48, no. 7, pp. 1872–1882, Jul. 2000.

[29] O. Besson, P. Stoica, and A. B. Gershman, "Simple and accurate direction of arrival estimator in the case of imperfect spatial coherence," *IEEE Trans. Signal Process.*, vol. 49, no. 4, pp. 730–737, Apr. 2001.

[30] D. Asztely, B. Ottersten, and A. L. Swindlehurst, "A generalized array manifold model for local scattering in wireless communications," in *Proc. IEEE Int. Conf. Acoust., Speech, Signal Process. (ICASSP)*, vol. 5. Apr. 1997, pp. 4021–4024.

[31] S. R. Lee, I. Song, T. Chang, and M. S. Lee, "Distributed source location estimation using a circular array," in *Proc. ISSPA*, Brisbane, QLD, Australia, Aug. 1996, pp. 341–344.

[32] Q. Wan and Y.-N. Peng, "Low-complexity estimator for four-dimensional parameters under a reparameterised distributed source model," *IEE Proc. Radar, Sonar Navigat.*, vol. 148, no. 6, pp. 313–317, Dec. 2001.

[33] S. R. Lee, I. Song, Y. U. Lee, and H. G. Kim, "Estimation of distributed elevation and azimuth angles using linear arrays," in *Proc. MILCOM*, McLean, VA, USA, Oct. 1996, pp. 868–872.

[34] X. Yang, G.-J. Li, and Z. Zheng, "Low-complexity 2D DOA estimator of coherently distributed noncircular sources," *Signal Process.*, vol. 83, no. 8, pp. 1789–1802, Aug. 2003.

[35] Z. Zheng, G. Li, and Y. Teng, "Low-complexity 2D DOA estimator for multiple coherently distributed sources," *Int. J. Comput. Math. Electr. Electron. Eng.*, vol. 31, no. 2, pp. 443–459, 2012.

[36] P. Ioannides and C. A. Balanis, "Uniform circular and rectangular arrays for adaptive beamforming applications," *IEEE Antennas Wireless Propag. Let.*, vol. 4, no. 1, pp. 351–354, Sep. 2005.

[37] B. Chen, Z. Zhong, B. Ai, and X. Chen, "Comparison of antenna arrays for MIMO system in high speed mobile scenarios," in *Proc. VTC Spring*, Yokohama, Japan, May 2011, pp. 1–5.

[38] M. D. Zoltowski, M. Haardt, and C. P. Mathews, "Closed-form 2-D angle estimation with rectangular arrays in element space or beamspace via unitary ESPRIT," *IEEE Trans. Signal Process.*, vol. 44, no. 2, pp. 316–328, Feb. 1996.

[39] I. S. Gradshteyn and I. M. Ryzhik, *Table of Integrals, Series, and Products*, 7th ed. Orlando, FL, USA: Academic, 2007.

[40] S. M. Kay, *Fundamentals Statistical Signal Processing: Estimation Theory*. Englewood Cliffs, NJ, USA: Prentice-Hall, 1993.

[41] G. H. Golub and C. F. Van Loan, *Matrix Computations*. Baltimore, ML, USA: The Johns Hopkins Univ. Press, 1996.

[42] B. N. Datta, *Numerical Linear Algebra and Applications*, 1st ed. Boston, MA, USA: Cengage Learning, 1995.

[43] C. Duofang, C. Baixiao, and Q. Guodong, "Angle estimation using ESPRIT in MIMO radar," *Electron. Lett.*, vol. 44, no. 12, pp. 770–771, Jun. 2008.

[44] R. Cao, X. Zhang, and F. Gao, "Propagator-based algorithm for localization of coherently distributed sources," in *Proc. 8th Int. Conf. WCSP*, Yangzhou, China, Oct. 2016, pp. 1–5.

YUAN ZHOU received the B.S. degree in information engineering from Beijing Institute of Technology (BIT), Beijing, China, in 2011. She is currently working toward the Ph.D. degree with the Research Institute of Communication Technology, BIT. Since 2014, she has been a Visiting Ph.D. Student with Prof. L. Hanzo and Prof. S. Chen with the School of Electronics and Computer Science, University of Southampton, U.K. Her research interests are in the areas of wireless communications and signal processing, including direction of arrival estimation, beamforming/precoding, signal detection, and coding.

ZESONG FEI (M'07–SM'16) received the Ph.D. degree in electronic engineering from Beijing Institute of Technology (BIT) in 2004. He is currently a Professor with the Research Institute of Communication Technology of BIT, where he is involved in the design of the next-generation high-speed wireless communication systems. His current research interests include wireless communications and multimedia signal processing. He is also a Principal Investigator of projects funded by the National Natural Science Foundation of China. He is a Senior Member of the Chinese Institute of Electronics and China Institute of Communications.

SHAOSHI YANG (S'09–M'13) received the B.Eng. degree in information engineering from Beijing University of Posts and Telecommunications, China, in 2006 and the Ph.D. degree in electronics and electrical engineering from University of Southampton, U.K., in 2013. From 2008 to 2009, he was involved in the Mobile WiMAX Standardization with Intel Labs China. From 2013 to 2016, he was a Research Fellow with the School of Electronics and Computer Science, University of Southampton. He is now a Full Professor with Beijing Institute of Technology, China. His research expertise include high-dimensional signal processing for 5G communications, green radio, heterogeneous networks, cross-layer interference management, mathematical optimization and its applications. He received the Dean's Award for Early Career Research Excellence from the University of Southampton. He is a member of the Isaac Newton Institute for Mathematical Sciences, Cambridge University. He was a Guest Associate Editor for IEEE JOURNAL ON SELECTED AREAS IN COMMUNICATIONS.

JINGMING KUANG received the B.S. and M.S. degrees in information and signal processing from Beijing Institute of Technology (BIT), Beijing, China, in 1966 and 1981, respectively, and the Ph.D. degree in electrical engineering from Technical University of Berlin, Berlin, Germany, in 1988. Since 1989, he has been a Professor with the School of Information and Electronics, BIT. He is the Founder of the BITCEricsson Research Center of Digital Communications, which was built in 1999. From 1993 to 2007, he was the Vice-President and the President of BIT. His research interests include theory and techniques of wireless communication and digital signal processing.

SHENG CHEN (M'90–SM'97–F'08) received the B.Eng. degree in control engineering from East China Petroleum Institute, Dongying, China, in 1982; the Ph.D. degree in control engineering from City University, London, in 1986; and the D.Sc. degree from University of Southampton, Southampton, U.K., in 2005.

From 1986 to 1999, he held research and academic appointments with The University of Sheffield, U.K.; The University of Edinburgh, U.K.; and University of Portsmouth, U.K. Since 1999, he has been with the School of Electronics and Computer Science, University of Southampton, where he holds the post of Professor in Intelligent Systems and Signal Processing. His research interests include adaptive signal processing, wireless communications, modeling and identification of nonlinear systems, neural network and machine learning, intelligent control system design, and evolutionary computation methods and optimization. He has authored over 550 research papers.

Dr. Chen is a Fellow of the United Kingdom Royal Academy of Engineering; a Fellow of IET; a Distinguished Adjunct Professor with King Abdulaziz University, Jeddah, Saudi Arabia; and an ISI Highly Cited Researcher in engineering (2004).

LAJOS HANZO (F'08) received the D.Sc. degree in electronics in 1976 and the Ph.D. degree in 1983. During his 40-year career in telecommunications he has held various research and academic posts in Hungary, Germany, and U.K. Since 1986, he has been with the School of Electronics and Computer Science, University of Southampton, U.K. He has successfully supervised 111 Ph.D. students. He is currently directing a 60-strong academic research team, working on a range of research projects in the field of wireless multimedia communications sponsored by industry, the Engineering and Physical Sciences Research Council, U.K., the European IST Programme, and the Mobile Virtual Centre of Excellence, U.K. His research is funded by the European Research Council's Senior Research Fellow Grant. He is an enthusiastic supporter of industrial and academic liaison and he offers a range of industrial courses. He has co-authored 18 John Wiley/IEEE Press books on mobile radio communications totalling in excess of 10 000 pages, and has published over 1600 research contributions on the IEEE Xplore web site. He has over 30 000 citations and an H-index of 67. He was FREng, FIET, and a Fellow of the EURASIP. In 2009, he received the honorary doctorate Doctor Honoris Causa from Technical University of Budapest and in 2015 from University of Edinburgh. He served as the TPC Chair and the General Chair of the IEEE conferences, presented keynote lectures and has been received a number of distinctions. He is also a Governor of the IEEE VTS. From 2008 to 2012, he was the Editor-in-Chief of IEEE Press and a Chaired Professor at Tsinghua University, Beijing. He is the Chair in telecommunications with University of Southampton.

● ● ●